

Nonlinear Perturbation Theory Integrated with Nonlocal Bias, Redshift-space Distortions, and Primordial Non-Gaussianity

Takahiko Matsubara*

*Kobayashi-Maskawa Institute for the Origin of Particles and the Universe,
Nagoya University, Chikusa, Nagoya, 464-8602, Japan; and
Department of Physics, Nagoya University, Chikusa, Nagoya, 464-8602, Japan*
(Dated: January 12, 2013)

The standard nonlinear perturbation theory of the gravitational instability is extended to incorporate the non-local bias, redshift-space distortions, and primordial non-Gaussianity. We show that local Eulerian bias is not generally compatible to local Lagrangian bias in nonlinear regime. The Eulerian and Lagrangian biases are nonlocally related order by order in the general perturbation theory. The relation between Eulerian and Lagrangian kernels of density perturbations with biasing are derived. The effects of primordial non-Gaussianity and redshift-space distortions are also incorporated in our general formalism, and diagrammatic methods are introduced. Vertex resummations of higher-order perturbations in the presence of bias are considered. Resummations of Lagrangian bias are shown to be essential to handle biasing schemes in a general framework.

PACS numbers: 98.80.-k, 98.65.-r

I. INTRODUCTION

The large-scale structure of the universe is one of the most powerful probes in cosmology. The statistical nature of primordial density fluctuations can be investigated by large-scale distributions of galaxies. Geometrical effects on the observed clustering pattern of galaxies can constrain the nature of dark energy, through the Alcock-Paczinski effect [1–3] or baryon acoustic oscillations (BAO) [4–6]. Recently, it is found that the presence of primordial non-Gaussianity introduces scale-dependent bias in the halo clustering [7–11]. Therefore, many possible models in cosmology, such as inflationary scenarios, dark energy models, modified gravity, and so on, should be constrained by precision measurements of the large-scale structure in near future.

To compare the observations with theory, it is crucial to make precise predictions of observable quantities from a given cosmological model. The linear theory applies on very large scales [12]. However, the linear theory is not sufficiently accurate for purposes in the precision cosmology.

Accurate predictions of statistical measures of galaxy clustering beyond the linear theory are provided by nonlinear theories. The method of numerical simulation is one of the most straightforward ways of investigating nonlinear dynamics. However, they are not free from numerical artefacts and systematics, such as finite-volume effects, finite-resolution effects, and so forth. Fortunately, the analytical perturbation theory is applicable on large scales where density fluctuations are small. Thus the nonlinear perturbation theory of gravitational instability attracts renewed interests in recent years.

The nonlinear perturbation theory have been developed since decades ago [13–20]. The traditional perturbation theory is formulated in Eulerian space, and such theory is referred to as the standard perturbation theory (SPT). The perturbation theory in Lagrangian space is also formulated [21–

29], which is called the Lagrangian perturbation theory (LPT). The first-order LPT corresponds to the classic Zel'dovich approximation [30].

In these years, the renormalized perturbation theory (RPT) [31, 32] and other approaches [33–39] have been developed to improve the accuracy of perturbation theory in nonlinear regime, partially taking into account higher-order effects of the SPT. Some of those approaches are based on the reformulation of fluid equations using the propagator, the vertex, and a source [40], which provides a way to use standard tools of field theory. Nevertheless, various levels of approximations and ansatz should be employed in those approaches.

The RPT and its variants mentioned above significantly improve the perturbation theory of dark matter in real space. However, one of the most important applications of the perturbation theory is to interpret the large-scale clustering of galaxies or other astronomical objects, observed by redshift surveys. The observable quantity in redshift surveys is the distribution of objects in redshift space. Even though the RPT and its variants could be powerful in predicting the nonlinear power spectrum of dark matter in real space, one could not directly compare the theoretical prediction with observations.

There are two obstacles to the comparison between the improved perturbation theories and observations. The first one is the redshift-space distortions: the redshift as a measure of the radial distance is contaminated by peculiar velocities. It is straightforward to take them into account in the SPT framework [41–44]. However, the SPT in redshift space breaks down at larger scales than in real space and the applicability range of scales is fairly narrow [44], since the SPT does not sufficiently reproduce the nonlinear smearing effects, known as the Fingers-of-God (FoG) effect [45, 46].

Nonlinear modelings of the redshift-space distortions beyond the SPT are proposed [47–49], in which the FoG effects are phenomenologically put by hand. It is found in those studies that the FoG effects can be represented by putting a Gaussian damping factor in front of the power spectrum. It is shown that the Gaussian damping factor in redshift space is naturally derived from the LPT [39], where the phenomeno-

*Electronic address: taka@a.phys.nagoya-u.ac.jp

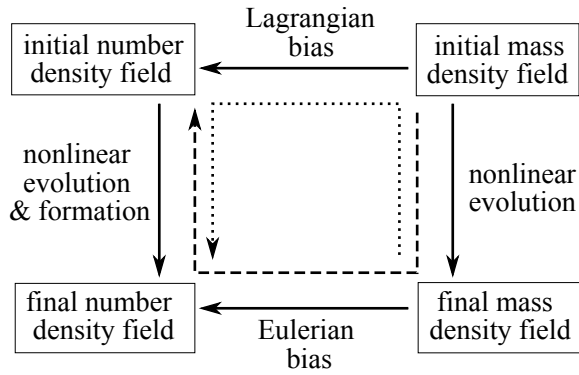


FIG. 1: The relation between Eulerian and Lagrangian biases. The Eulerian bias is expressible by the Lagrangian bias (dotted arrow) and vice versa (dashed arrow), only when the biases are allowed to be nonlocal. Note that nonlinear evolutions and formation of objects are nonlocal processes in nonlinear regime.

logical Gaussian factor should be modified and additional mode-coupling terms should be taken into account in nonlinear redshift space.

The second obstacle to the comparison between perturbation theories and observations is the biasing. Any astronomical objects which can be observed are biased tracers of underlying mass distributions. In the galaxy redshift surveys, the tracers are galaxies. The exact relationship between the distribution of mass and that of galaxies depends on the complex, nonlinear process of galaxy formation which is not clearly understood.

Analytic models of biasing have been proposed, including the model of local Eulerian bias [50–52], the halo model [53–57], peaks model [58–64], etc. The first model is a purely phenomenological parameterization of the bias, assuming a local relation between the mass and galaxy distributions. The last two models are relatively more physical than the first one, and are categorized as the Lagrangian bias, i.e., the locations of the galaxy formation are specified in initial density fields. The location of a peak, for example, is displaced by the dynamical evolution of density fluctuations. In the framework of SPT, the local Eulerian bias is usually adopted [43, 44, 65–67]. However, as shown below in this paper, the halo model and the peaks model are not compatible with the local Eulerian bias in nonlinear regime, because the gravitational evolutions are nonlocal process in general.

In Fig. 1, the relation between the Eulerian and Lagrangian biases is shown. The final mass density field is the result of nonlinear evolutions from the initial mass density field. The final number density field of objects, which are observable such as galaxies, is the result of nonlinear evolutions and formations of those objects. The sites of the formation in Lagrangian space define the initial number density field. Thus the initial number density field also depends on the redshift of observation. The Lagrangian bias corresponds to the relation between the initial mass density field and the initial number density field, while the Eulerian bias corresponds to the relation between the final mass density field and the final number

density field.

The initial number density field is constructed only when the formation process is known. For example, the halo model and the peaks model give prescriptions of constructing the initial number density field from the initial mass density field; i.e., these models specify the Lagrangian bias. In the halo model with the peak-background split [53], the initial number density is locally determined by initial mass density field. Thus the halo model corresponds to a local Lagrangian bias. In the peaks model, the sites of the formation is not locally determined, since the peaks are defined not only by local values, but also by spatial derivatives of the field [60]. Thus the peaks model corresponds to a (semi-)nonlocal Lagrangian bias. Such models of Lagrangian bias are more physically motivated than the Eulerian bias. The bias depends on the properties of observed objects, such as the mass and luminosity. The Lagrangian bias schemes described above actually depend on the mass (or the peak height) of collapsed objects.

The local Lagrangian bias and the local Eulerian bias are not compatible to each other in nonlinear regime. This fact is well illustrated in Fig. 1. The Eulerian bias is expressible by the Lagrangian bias (dashed arrow) and vice versa (dotted arrow). The relations involves nonlinear evolutions of mass, and nonlinear evolutions and formation of observed objects. Nonlinear evolutions and formations are nonlocal processes. Therefore, the Eulerian bias should be nonlocal even when the Lagrangian bias is local. The local biasing schemes are compatible only in the case that the linear theory and a local approximation of formation process are valid. Such conditions do not apply in generally nonlinear regime.

In reality, the bias is definitely nonlocal. For example, the galaxies are largely affected by their environment [68]. The nonlocality should be taken into account in a precise modeling of the bias. The exact forms of the nonlocality in formation processes of observed objects have not been fully understood. It requires a lot of future work with analytic, numerical, and observational studies of complicated astrophysical processes to understand the exact nonlocality of bias.

One of the main purposes of this paper is to formulate a nonlinear perturbation theory which can handle both the Eulerian and Lagrangian nonlocal biases in general. There mainly two merits in this formulation. First, one can distinguish general properties of nonlinear clustering which do not depend on details of formation processes from those which largely depends on models of bias. Second, it is straightforward to predict observable quantities in any models of bias. Effects of redshift-space distortions and primordial non-Gaussianity are also included in the formalism. Resummation techniques in the presence of nonlocal bias are introduced as well. The resummations of bias are shown to be essential to handle the nonlocal bias in a general way.

This paper is organized as follows. In Sec. II, both Eulerian and Lagrangian perturbation theories in real space are extended to include both the nonlocal bias and the primordial non-Gaussianity. Diagrammatic methods with graphical representations are introduced. The relation between the perturbative kernels of EPT and LPT with nonlocal bias is derived as well. In Sec. III, the formalism of the previous sec-

tion is extended to include the effect of redshift-space distortions. Techniques of the vertex resummations in our formalism are introduced in Sec. IV, and finally, some models of the Lagrangian bias are considered, illustrating how higher-order bias factors are evaluated in our formalism.

II. NONLINEAR PERTURBATION THEORY WITH NONLOCAL BIAS

A. Nonlocal bias in Eulerian space

In the following, the density contrast of observed objects X at a comoving, Eulerian position \mathbf{x} is denoted by $\delta_X(\mathbf{x})$. The observed objects X can be any astronomical objects such as galaxies, quasars, absorption lines, 21cm emissions, and so forth, which are selected and catalogued in a given redshift survey. The density field of the objects is not generally a local nor linear function of the underlying mass density contrast $\delta_m(\mathbf{x})$. Instead, they are nonlocally and nonlinearly related to each other in general. In other words, the density contrast δ_X of objects is a functional of the mass density contrast δ_m .

The functional relation between density fields of mass and objects is deterministic on scales we are interested in. One might think that the formation process of objects is determined not only by the density field of mass, but also by other physical factors such as the local radiation density and its spectrum, merger histories of galaxies, etc. However, the dynamical evolutions in the structure formation are deterministic, and the initial density field uniquely determines all the subsequent states of the universe, including the above complex factors. Consequently, when only the growing mode solutions are kept, density contrasts of mass and objects are nonlocal functionals of initial density contrast δ_L : we have $\delta_m = \mathcal{F}_m[\delta_L]$ and $\delta_X = \mathcal{F}_X[\delta_L]$, where \mathcal{F}_m and \mathcal{F}_X represent nonlocal functionals.

On scales where the perturbation theory is applicable, the motion of dark matter is single streaming. In which case, the spatial distribution of dark matter uniquely inverted to give the initial density field $\delta_L = \mathcal{F}_m^{-1}[\delta_m]$. Thus we have a deterministic functional relation $\delta_X[\delta_m] = \mathcal{F}_X[\mathcal{F}_m^{-1}[\delta_m]]$. Taking into account the translational invariance, the Taylor expansion of the functional is generally given by

$$\delta_X(\mathbf{x}) = \sum_{n=0}^{\infty} \frac{1}{n!} \int d^3x_1 \cdots d^3x_n b_n(\mathbf{x} - \mathbf{x}_1, \dots, \mathbf{x} - \mathbf{x}_n) \times \delta_m(\mathbf{x}_1) \cdots \delta_m(\mathbf{x}_n). \quad (1)$$

The nonlocal bias functions, $\{b_n\}$, specify the relation between the number density field of objects and mass density field. The first term with $n = 0$ in Eq. (1) gives just a constant b_0 , which is determined by other functions b_n to ensure a condition $\langle \delta_X \rangle = 0$. The constant term b_0 is irrelevant as we consider connected moments of the density contrast. In Fourier space, moreover, the constant term just disappears when nonzero modes $\mathbf{k} \neq \mathbf{0}$ are considered. Therefore, we do not retain the constant term b_0 in the below.

The Taylor expansion of Eq. (1) is applicable only when the functional dependence is smooth. However, as shown in Sec. IV below, the technique of vertex resummation relaxes this constraint, and even singular dependences of the number density field on the mass density field can be handled with this technique.

The local biasing ansatz is recovered when $b_n(\mathbf{x}_1, \dots, \mathbf{x}_n)$ is replaced by $W_R(\mathbf{x}_1) \cdots W_R(\mathbf{x}_n) b_n$, where b_n is now a constant for each n , and $W_R(\mathbf{x})$ is a smoothing kernel with a smoothing radius of R . However, the Eulerian local biasing scheme is not a natural model when we consider nonlinear dynamics, as we explicitly show below in this paper.

In Fourier space, Eq. (1) reduces to

$$\delta_X(\mathbf{k}) = \sum_{n=1}^{\infty} \frac{1}{n!} \int \frac{d^3k_1}{(2\pi)^3} \cdots \frac{d^3k_n}{(2\pi)^3} (2\pi)^3 \delta_D^3(\mathbf{k}_{1\dots n} - \mathbf{k}) \times b_n(\mathbf{k}_1, \dots, \mathbf{k}_n) \delta_m(\mathbf{k}_1) \cdots \delta_m(\mathbf{k}_n), \quad (2)$$

where we use a notation,

$$\mathbf{k}_{1\dots n} \equiv \mathbf{k}_1 + \cdots + \mathbf{k}_n, \quad (3)$$

throughout this paper. Some variables like δ_m , δ_X and b_n in Fourier space are denoted by the same symbols as those in real space, instead of properly using symbols like $\tilde{\delta}_m$, $\tilde{\delta}_X$, \tilde{b}_n , etc. We will work in Fourier space in most of this paper. The convention of Fourier transform and its inverse in this paper is given by

$$\tilde{F}(\mathbf{k}) = \int d^3x e^{-i\mathbf{k}\cdot\mathbf{x}} F(\mathbf{x}), \quad \tilde{F}(\mathbf{x}) = \int \frac{d^3k}{(2\pi)^3} e^{i\mathbf{k}\cdot\mathbf{x}} \tilde{F}(\mathbf{k}). \quad (4)$$

Since the bias relations should not depend on the coordinates system, the bias functions b_n should be rotationally invariant. For example, the first-order bias function $b_1(\mathbf{k})$ is actually a function of the magnitude $k = |\mathbf{k}|$ and can be denoted as $b_1(k)$. Similarly, the second-order bias function $b_2(\mathbf{k}_1, \mathbf{k}_2)$ is actually a function of k_1 , k_2 , and $k_{12} = |\mathbf{k}_1 + \mathbf{k}_2|$ which characterize relative configuration of \mathbf{k}_1 and \mathbf{k}_2 . Thus the function can be denoted as $b_2(k_1, k_2; k_{12})$, where the first two arguments are symmetric under a permutation, but the last one. Similarly, the third-order bias function can be denoted as $b_3(k_1, k_2, k_3; k_{12}, k_{23}, k_{31})$, and higher-order bias functions depend only on rotationally invariant set of variables.

In the case of local biasing ansatz, $b_n(\mathbf{k}_1, \dots, \mathbf{k}_n)$ is replaced by $W(k_1 R) \cdots W(k_n R) b_n$, where b_n is now a constant for each n , and $W(kR)$ is a smoothing window function. When the smoothing radius R is much smaller than the clustering scales we are interested in, the smoothing window function can be dropped and each bias function is simply considered as a constant b_n in Fourier space.

The mass density contrast $\delta_m(\mathbf{x})$ is also a nonlocal and nonlinear functional of a linear density field $\delta_L(\mathbf{x})$. We have a Taylor expansion which has a similar form with Eq. (2) in Fourier space:

$$\delta_m(\mathbf{k}) = \sum_{n=1}^{\infty} \frac{1}{n!} \int \frac{d^3k_1}{(2\pi)^3} \cdots \frac{d^3k_n}{(2\pi)^3} (2\pi)^3 \delta_D^3(\mathbf{k}_{1\dots n} - \mathbf{k}) \times F_n(\mathbf{k}_1, \dots, \mathbf{k}_n) \delta_L(\mathbf{k}_1) \cdots \delta_L(\mathbf{k}_n), \quad (5)$$

where F_n 's are perturbative kernels. We consider the density fields at any given redshift, and time-dependences are suppressed in the above notations. For the linear density field, $\delta_L(\mathbf{k}) = D(z)\delta_0(\mathbf{k})$, where $D(z)$ is the linear growth factor at a redshift z , and $\delta_0(\mathbf{k})$ is the linear density contrast at the present time $z = 0$. We adopt a normalization $D(z = 0) = 1$ in this paper.

The evolution of the mass density field can be evaluated perturbatively in quasi-nonlinear regime. The SPT evaluates the perturbative kernel F_n in Eulerian space order by order [15, 16, 18, 20]. For $n = 1, 2$, for example, we have

$$F_1(\mathbf{k}) = 1, \quad (6)$$

$$F_2(\mathbf{k}_1, \mathbf{k}_2) = \frac{10}{7} + \left(\frac{k_1}{k_2} + \frac{k_2}{k_1}\right) \frac{\mathbf{k}_1 \cdot \mathbf{k}_2}{k_1 k_2} + \frac{4}{7} \left(\frac{\mathbf{k}_1 \cdot \mathbf{k}_2}{k_1 k_2}\right)^2. \quad (7)$$

Expressions of F_3 and F_4 are explicitly given in Ref. [16]. Although above kernels F_n ($n \geq 2$) are exact only in the Einstein-de Sitter universe, $\Omega_M = 1$, $\Omega_\Lambda = 0$, those are good approximations in other cosmological models with $\Omega_M \neq 1$, $\Omega_\Lambda \neq 0$ [20].

Combining Eq. (2) and Eq. (5), we have a formal expansion of the form

$$\delta_X(\mathbf{k}) = \sum_{n=1}^{\infty} \frac{1}{n!} \int \frac{d^3 k_1}{(2\pi)^3} \cdots \frac{d^3 k_n}{(2\pi)^3} (2\pi)^3 \delta_D^3(\mathbf{k}_{1\dots n} - \mathbf{k}) \times K_n(\mathbf{k}_1, \dots, \mathbf{k}_n) \delta_L(\mathbf{k}_1) \cdots \delta_L(\mathbf{k}_n), \quad (8)$$

where

$$K_1(\mathbf{k}) = b_1(\mathbf{k}), \quad (9)$$

$$K_2(\mathbf{k}_1, \mathbf{k}_2) = b_1(\mathbf{k})F_2(\mathbf{k}_1, \mathbf{k}_2) + b_2(\mathbf{k}_1, \mathbf{k}_2) \quad (10)$$

$$K_3(\mathbf{k}_1, \mathbf{k}_2, \mathbf{k}_3) = b_1(\mathbf{k})F_3(\mathbf{k}_1, \mathbf{k}_2, \mathbf{k}_3) + [b_2(\mathbf{k}_1, \mathbf{k}_{23})F_2(\mathbf{k}_2, \mathbf{k}_3) + \text{cyc.}] + b_3(\mathbf{k}_1, \mathbf{k}_2, \mathbf{k}_3), \quad (11)$$

and so forth, where $\mathbf{k} = \mathbf{k}_{1\dots n}$ in each expression of K_n .

The N -point polyspectrum $P_X^{(N)}$ of the field δ_X is defined by

$$\langle \delta_X(\mathbf{k}_1) \cdots \delta_X(\mathbf{k}_N) \rangle_c = (2\pi)^3 \delta_D^3(\mathbf{k}_{1\dots N}) P_X^{(N)}(\mathbf{k}_1, \dots, \mathbf{k}_N), \quad (12)$$

where $\langle \cdots \rangle_c$ denotes the cumulant, which corresponds to the connected part of the N -point expectation value. The 2-point polyspectrum is the power spectrum $P_X = P_X^{(2)}$. The 3- and 4-point polyspectra are the bispectrum $B_X = P_X^{(3)}$ and the trispectrum $T_X = P_X^{(4)}$, respectively. Substituting the Eq. (8) into Eq. (12), one can perturbatively evaluate the polyspectra $P_X^{(N)}$ in terms of the polyspectra $P_L^{(n)}$ of the linear density contrast δ_L , which is similarly defined by

$$\langle \delta_L(\mathbf{k}_1) \cdots \delta_L(\mathbf{k}_n) \rangle_c = (2\pi)^3 \delta_D^3(\mathbf{k}_{1\dots n}) P_L^{(n)}(\mathbf{k}_1, \dots, \mathbf{k}_n). \quad (13)$$

The linear polyspectra $P_L^{(n)}$ are proportional to the primordial spectra. When the initial density field is random Gaussian, only the primordial power spectrum is present and higher-order linear polyspectra all vanish.

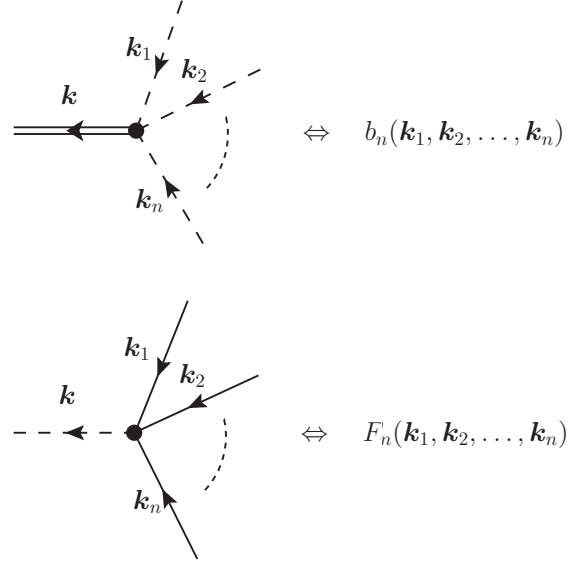


FIG. 2: Diagrammatic rules for the Eulerian perturbation theory in real space. In each vertex, $\mathbf{k} = \mathbf{k}_1 + \cdots + \mathbf{k}_n$ should be satisfied. The upper and lower rules correspond to the expansions in Eq. (2) and (5), respectively. A dashed line should be “internal”: one end of a dashed line should be connected to a vertex with double solid line, and the other end should be connected to a vertex with solid lines.

In calculating the polyspectra, diagrammatic methods are quite useful. Fig. 2 shows the diagrammatic rules for the Eulerian perturbation theory in real space. The first rule corresponds to each term in the expansion of Eq. (2), and the second rule corresponds to each term in Eq. (5). In both vertices, a momentum conservation $\mathbf{k} = \mathbf{k}_1 + \cdots + \mathbf{k}_n$ should be satisfied, according to the Dirac's delta function in each corresponding equation. The double solid line, dashed line, and single solid line correspond to δ_X , δ_m , and δ_L , respectively. Since the variable δ_m is expanded according to Eq. (5), dashed lines in the upper rule should always be connected to the vertices of the lower rule, i.e., the dashed lines are “internal.”

To evaluate the N -point polyspectra of Eq. (12) with expansions of Eqs. (2) and (5), we need cumulants of the linear density contrast δ_L , which are given by Eq. (13). This procedure is diagrammatically equivalent to applying rules in Fig. 3. The open circles with cross represent the primordial polyspectra. When the initial density field is random Gaussian, higher-order polyspectra all vanish, $P_L^{(n)} = 0$ for $n \geq 3$, and only the upper rule in Fig. 3 is relevant.

For the evaluations of N -point polyspectra $P_X^{(N)}$ in Eq. (12), we first consider N vertices with double solid lines. Next we consider possible ways of connecting those vertices with dashed lines and solid lines according to the rules in Figs. 2 and 3. The polyspectra $P_X^{(N)}$ is given by the sum of terms which correspond to all the possible diagrams, with appropriate statistical factors which are explained at the end of this subsection.

Since the N -point polyspectra are defined by the connected part in Eq. (12), only connected diagrams should be taken

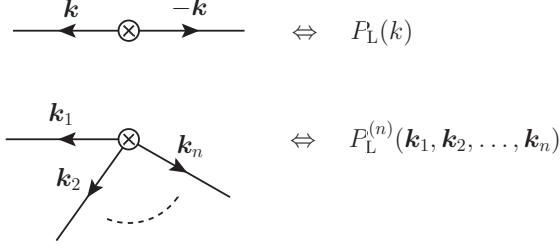


FIG. 3: Diagrammatic rules for contributions from the primordial polyspectra. All the free ends of solid lines in Fig. 2 should be connected to each other by these rules. When the initial density field is random Gaussian, the lower graph with $n \geq 3$ does not exist. In the lower graph, $\mathbf{k}_1 + \dots + \mathbf{k}_n = \mathbf{0}$ should be satisfied. The case of $n = 2$ in the lower graph is equivalent to the upper graph.

into account. Discarding unconnected diagrams is equivalent to taking the connected part. When there exist internal wavevectors $\mathbf{k}'_1, \mathbf{k}'_2, \dots$, which are not uniquely determined from external wavevectors $\mathbf{k}_1, \dots, \mathbf{k}_N$, those internal wavevectors should be integrated with a weight of $(2\pi)^{-3}$, i.e., $\int d^3k'_1/(2\pi)^3 \cdot d^3k'_2/(2\pi)^3 \dots$. The number of internal wavevectors to be integrated is the same as the number of loops in a given diagram.

Every terms in the perturbative expansion of the polyspectra $P_X^{(N)}$ of Eq. (12) corresponds to the diagrams constructed by above rules. When the hierarchical orders for the linear polyspectra $P_L^{(N)} \sim O(P_L)^{N-1}$ hold, the number of loops is equal to the order of P_L in a given diagram. In any case, the perturbative order in a given diagram is apparent from the number and kind of crossed circles.

When the mixed polyspectra of different types of objects, such as cross power spectra $P_{mX}(k)$, $P_{X_1X_2}(k)$, etc., are need to be evaluated, we just use different vertices with corresponding set of bias functions.

When the bias is not present, $b_1 = 1, b_2 = b_3 = \dots = 0$, only one dashed line can be connected to each vertex of the lower rule in Fig. 2. In this case one does not need to consider the dashed line at all, and the diagrammatic rules of Figs. 2 and 3 are equivalent to the ones which were previously introduced in Ref. [16], in which Gaussian initial conditions are assumed. Therefore, our diagrammatic rules of Figs. 2 and 3 are generalization of the previous rules to the case when the Eulerian nonlocal bias and primordial non-Gaussianity are present in general.

The diagrammatic rule for the expansion of Eq. (8) is shown in Fig. 4. The triangle vertex corresponds to shrinking the vertex in terms of the diagrammatic rules of Fig. 2. In fact, for $n = 1, 2, 3$, the shrunk vertices are diagrammatically given by Fig. 5. These diagrammatic representations are equivalent to Eqs. (9)–(11).

As an example, Fig. 6 shows diagrams for the power spectrum up to the one-loop order in terms of shrunk vertices. It is a good exercise for readers to explicitly calculate the power spectrum from Eqs. (8) and (12), without resorting diagrams, and compare the result with the diagrammatic representation

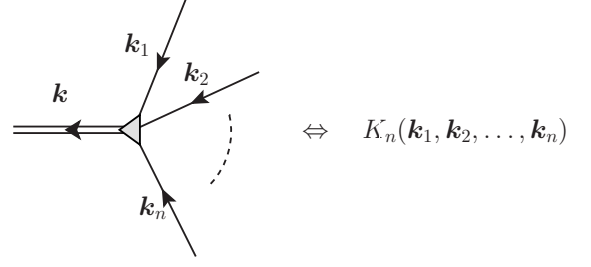


FIG. 4: Shrunk vertex. The triangle represents all the possible tree graphs constructed by the rules in Fig. 2 of EPT. The shrunk vertex can also be expressed by LPT diagrams.

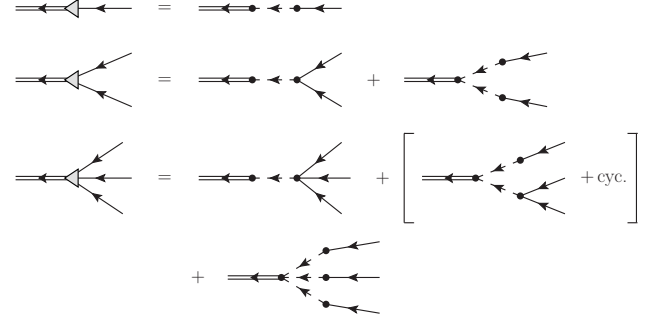


FIG. 5: Shrunk vertices in Eulerian perturbation theory in real space.

of Fig. 6. The result is given by

$$\begin{aligned}
 P_X(k) &= [K_1(k)]^2 P_L(k) \\
 &+ \frac{1}{2} \int \frac{d^3k'}{(2\pi)^3} [K_2(\mathbf{k}', \mathbf{k} - \mathbf{k}')]^2 P_L(k') P_L(|\mathbf{k} - \mathbf{k}'|) \\
 &+ K_1(k) P_L(k) \int \frac{d^3k'}{(2\pi)^3} K_3(\mathbf{k}, \mathbf{k}', -\mathbf{k}') P_L(k') \\
 &+ K_1(k) \int \frac{d^3k'}{(2\pi)^3} K_2(\mathbf{k}', \mathbf{k} - \mathbf{k}') B_L(\mathbf{k}, \mathbf{k}' - \mathbf{k}, -\mathbf{k}'). \quad (14)
 \end{aligned}$$

One should be careful to put a correct statistical factor in each diagram. When there are equivalent pieces in a diagram, one should put a statistical factor $1/n_{\text{equiv}}!$, where n_{equiv} is the number of that equivalent pieces. For example, the second diagram in Fig. 6 has a pair of equivalent lines connecting

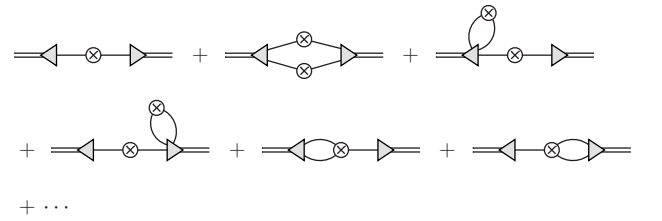


FIG. 6: Diagrams up to one-loops for the power spectrum.

both vertices. It has a two equivalent pieces, and the resulting statistical factor is $1/2! = 1/2$. In another way of viewing the statistical factor of this diagram, each vertex has a factor $1/2!$ because of the prefactor $1/n!$ in Eq. (8), and there is two ways of connecting the solid lines from the vertices, resulting in the final statistical factor of $(1/2!)^2 \times 2 = 1/2$, which agrees with the previous consideration of equivalent pieces. In the third diagram, two solid lines in the loop connected to the left vertex are equivalent pieces, and the statistical factor is $1/2! = 1/2$. In another way of viewing, left vertex has a factor $1/3!$, and there are three ways of choosing which solid lines are associated to the loop, resulting in the final statistical factor of $1/3! \times 3 = 1/2$, which agrees with the previous consideration of equivalent pieces. The fourth diagram gives the same expression with the third, due to the parity symmetry. Similarly, the fifth and sixth diagrams have the statistical factor of $1/2! = 1/2$ in both ways of viewing. After some experience, one can put a correct statistical factor in a given diagram. Two ways of counting as in the above examples are helpful for cross-checking.

B. Nonlocal bias in Lagrangian space

In the Lagrangian view, the dynamical evolution of cosmological density fields is tracked by a set of trajectories of mass element, $\mathbf{x}(\mathbf{q}, t)$, where \mathbf{q} is the initial Lagrangian coordinates of the trajectory. A displacement field $\Psi(\mathbf{q}, t)$ is defined by

$$\mathbf{x}(\mathbf{q}, t) = \mathbf{q} + \Psi(\mathbf{q}, t), \quad (15)$$

and is considered as a fundamental quantity in the Lagrangian view of perturbations.

Since the initial density field is sufficiently uniform, the Eulerian mass density field $\rho_m(\mathbf{x})$ satisfies the continuity relation,

$$\rho_m(\mathbf{x})d^3x = \bar{\rho}_m d^3q, \quad (16)$$

where $\bar{\rho}_m$ is the comoving mean density of mass. On the other hand, the fluid elements in which observed objects reside are not uniformly distributed in Lagrangian space. The continuity relation is given by

$$\rho_X(\mathbf{x})d^3x = \rho_X^L(\mathbf{q})d^3q, \quad (17)$$

where $\rho_X^L(\mathbf{q})$ is the density field of the observed objects in Lagrangian space. Note that both ρ_X and ρ_X^L depend on the time of observation, because objects are identified by observers at a given time. The comoving mean density of the objects, $\bar{\rho}_X$ is common to both density fields, and the Eq. (17) is equivalent to the following equation:

$$1 + \delta_X(\mathbf{x}) = \int d^3q \left[1 + \delta_X^L(\mathbf{q}) \right] \delta_D^3[\mathbf{x} - \mathbf{q} - \Psi(\mathbf{q})]. \quad (18)$$

When the density field is not biased, $\delta_X^L(\mathbf{q}) = 0$ everywhere.

The expansion of the number density field by the linear density field in Lagrangian space is formally given by

$$\delta_X^L(\mathbf{k}) = \sum_{n=1}^{\infty} \frac{1}{n!} \int \frac{d^3k_1}{(2\pi)^3} \cdots \frac{d^3k_n}{(2\pi)^3} (2\pi)^3 \delta_D^3(\mathbf{k}_{1\dots n} - \mathbf{k}) \times b_n^L(\mathbf{k}_1, \dots, \mathbf{k}_n) \delta_L(\mathbf{k}_1) \cdots \delta_L(\mathbf{k}_n), \quad (19)$$

where b_n^L is the n -th order nonlocal bias function in Lagrangian space. The bias functions are essentially infinite-dimensional Taylor coefficients, and given by functional derivatives:

$$b_n^L(\mathbf{k}_1, \dots, \mathbf{k}_n) = (2\pi)^{3n} \int \frac{d^3k'}{(2\pi)^3} \frac{\delta^n \delta_X^L(\mathbf{k}')}{\delta \delta_L(\mathbf{k}_1) \cdots \delta \delta_L(\mathbf{k}_n)} \Big|_{\delta_L=0}. \quad (20)$$

Applying the Fourier transform to the Eq. (18), and expanding the exponent of the displacement field, we have

$$\begin{aligned} \delta_X(\mathbf{k}) &= \int d^3q e^{-ik \cdot \mathbf{q}} \left[1 + \delta_X^L(\mathbf{q}) \right] e^{-ik \cdot \Psi(\mathbf{q})} - (2\pi)^3 \delta_D^3(\mathbf{k}) \\ &= \sum_{n+m \geq 1} \frac{(-i)^m}{n!m!} \int \frac{d^3k_1}{(2\pi)^3} \cdots \frac{d^3k_n}{(2\pi)^3} \frac{d^3k'_1}{(2\pi)^3} \cdots \frac{d^3k'_m}{(2\pi)^3} \\ &\quad \times (2\pi)^3 \delta_D^3(\mathbf{k}_{1\dots n} + \mathbf{k}'_{1\dots m} - \mathbf{k}) b_n^L(\mathbf{k}_1, \dots, \mathbf{k}_n) \\ &\quad \times \delta_L(\mathbf{k}_1) \cdots \delta_L(\mathbf{k}_n) [\mathbf{k} \cdot \tilde{\Psi}(\mathbf{k}'_1)] \cdots [\mathbf{k} \cdot \tilde{\Psi}(\mathbf{k}'_m)], \end{aligned} \quad (21)$$

where we define $b_0^L \equiv 1$ above just for $n = 0$, and $\tilde{\Psi}$ is the Fourier transform of the displacement field. In the following we use the displacement field both in configuration space and Fourier space, and we notationally distinguish between Ψ and $\tilde{\Psi}$.

The displacement field Ψ is similarly expanded in Lagrangian space:

$$\begin{aligned} \tilde{\Psi}(\mathbf{k}) &= \sum_{n=1}^{\infty} \frac{i}{n!} \int \frac{d^3k_1}{(2\pi)^3} \cdots \frac{d^3k_n}{(2\pi)^3} (2\pi)^3 \delta_D^3(\mathbf{k}_{1\dots n} - \mathbf{k}) \\ &\quad \times \mathbf{L}_n(\mathbf{k}_1, \dots, \mathbf{k}_n) \delta_L(\mathbf{k}_1) \cdots \delta_L(\mathbf{k}_n). \end{aligned} \quad (22)$$

The evolution of the displacement field can be perturbatively evaluated in quasi-nonlinear regime. The LPT evaluates the perturbative kernel \mathbf{L}_n order by order [27, 28, 39]. For $n = 1, 2$, we have

$$\mathbf{L}_1(\mathbf{k}) = \frac{\mathbf{k}}{k^2}, \quad (23)$$

$$\mathbf{L}_2(\mathbf{k}_1, \mathbf{k}_2) = \frac{3}{7} \frac{\mathbf{k}}{k^2} \left[1 - \left(\frac{\mathbf{k}_1 \cdot \mathbf{k}_2}{k_1 k_2} \right)^2 \right], \quad (24)$$

where $\mathbf{k} = \mathbf{k}_1 + \mathbf{k}_2$ for \mathbf{L}_2 . As in Eq. (7), the above kernel \mathbf{L}_2 is exact only for Einstein–de-Sitter universe, and the expression is a good approximation in other cosmological models. The explicit form of the third-order kernel \mathbf{L}_3 is given in [27]. The kernel \mathbf{L}_n is not proportional to \mathbf{k} for $n \geq 3$, in general.

Diagrammatic rules for Eqs. (21) and (22) are given in Fig. 7. The double solid line and single solid line correspond to δ_X and δ_L , respectively. The wavy line correspond to the n -th order perturbation of the displacement vector Ψ , and has an index i which corresponds to a component of the vector. The wavy lines also carry wavevectors, and momentum conservations should be satisfied at every vertices.

Combining Eqs. (21) and (22), we have a formal expansion which should be identical to the Eq. (8) in EPT. The first sev-

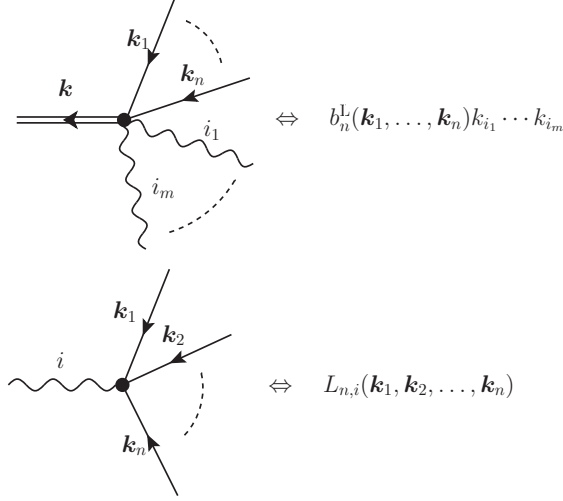


FIG. 7: Diagrammatic rules for the Lagrangian perturbation theory in real space. The symbols k_i and $L_{n,i}$ are i -components of \mathbf{k} and \mathbf{L}_n , respectively. The wavy lines are internal, and also carry wavevectors. The momentum conservation should be satisfied at each vertex. The diagrammatic rules in redshift space are just given by replacements $L_n \rightarrow L_n^s$

eral kernels are given by

$$K_1(\mathbf{k}) = \mathbf{k} \cdot \mathbf{L}_1(\mathbf{k}) + b_1^L(\mathbf{k}), \quad (25)$$

$$K_2(\mathbf{k}_1, \mathbf{k}_2) = \mathbf{k} \cdot \mathbf{L}_2(\mathbf{k}_1, \mathbf{k}_2) + [\mathbf{k} \cdot \mathbf{L}_1(\mathbf{k}_1)][\mathbf{k} \cdot \mathbf{L}_1(\mathbf{k}_2)] + b_1^L(\mathbf{k}_1)[\mathbf{k} \cdot \mathbf{L}_1(\mathbf{k}_2)] + b_1^L(\mathbf{k}_2)[\mathbf{k} \cdot \mathbf{L}_1(\mathbf{k}_1)] + b_2^L(\mathbf{k}_1, \mathbf{k}_2), \quad (26)$$

$$K_3(\mathbf{k}_1, \mathbf{k}_2, \mathbf{k}_3) = \mathbf{k} \cdot \mathbf{L}_3(\mathbf{k}_1, \mathbf{k}_2, \mathbf{k}_3) + \{[\mathbf{k} \cdot \mathbf{L}_1(\mathbf{k}_1)][\mathbf{k} \cdot \mathbf{L}_2(\mathbf{k}_2, \mathbf{k}_3)] + \text{cyc.}\} + [\mathbf{k} \cdot \mathbf{L}_1(\mathbf{k}_1)][\mathbf{k} \cdot \mathbf{L}_1(\mathbf{k}_2)][\mathbf{k} \cdot \mathbf{L}_1(\mathbf{k}_3)] + \{b_1^L(\mathbf{k}_1)[\mathbf{k} \cdot \mathbf{L}_2(\mathbf{k}_2, \mathbf{k}_3)] + \text{cyc.}\} + \{b_1^L(\mathbf{k}_1)[\mathbf{k} \cdot \mathbf{L}_1(\mathbf{k}_2)][\mathbf{k} \cdot \mathbf{L}_1(\mathbf{k}_3)] + \text{cyc.}\} + \{b_2^L(\mathbf{k}_1, \mathbf{k}_2)[\mathbf{k} \cdot \mathbf{L}_1(\mathbf{k}_3)] + \text{cyc.}\} + b_3^L(\mathbf{k}_1, \mathbf{k}_2, \mathbf{k}_3) \quad (27)$$

and so forth, where $\mathbf{k} = \mathbf{k}_{1\dots n}$ for K_n . Those equations are diagrammatically represented in Fig. 8.

When the bias is not present, $b_1 = 1$, $b_1^L = 0$, and $b_n = b_n^L = 0$ for $n \geq 2$. In this case, the equivalence of Eqs. (9)–(11) and Eqs. (25)–(27) indicates

$$F_1(\mathbf{k}) = \mathbf{k} \cdot \mathbf{L}_1(\mathbf{k}), \quad (28)$$

$$F_2(\mathbf{k}_1, \mathbf{k}_2) = \mathbf{k} \cdot \mathbf{L}_2(\mathbf{k}_1, \mathbf{k}_2) + [\mathbf{k} \cdot \mathbf{L}_1(\mathbf{k}_1)][\mathbf{k} \cdot \mathbf{L}_1(\mathbf{k}_2)], \quad (29)$$

$$F_3(\mathbf{k}_1, \mathbf{k}_2, \mathbf{k}_3) = \mathbf{k} \cdot \mathbf{L}_3(\mathbf{k}_1, \mathbf{k}_2, \mathbf{k}_3) + \{[\mathbf{k} \cdot \mathbf{L}_1(\mathbf{k}_1)][\mathbf{k} \cdot \mathbf{L}_2(\mathbf{k}_2, \mathbf{k}_3)] + \text{cyc.}\} + [\mathbf{k} \cdot \mathbf{L}_1(\mathbf{k}_1)][\mathbf{k} \cdot \mathbf{L}_1(\mathbf{k}_2)][\mathbf{k} \cdot \mathbf{L}_1(\mathbf{k}_3)], \quad (30)$$

and so forth, where $\mathbf{k} = \mathbf{k}_{1\dots n}$ for F_n . The above equations give the relations of kernels in Lagrangian and Eulerian perturbation theories for dark matter evolutions. Therefore, those equations are identities. It is easily seen that Eqs. (28), (29) explicitly hold for Eqs. (6), (7), (23), (24).

C. The relation between Eulerian and Lagrangian bias functions

In the presence of bias, the equivalence of Eqs. (9)–(11) and Eqs. (25)–(27) indicates the relation between the Eulerian and Lagrangian bias. First several relations are given by

$$b_1(\mathbf{k}) = b_1^L(\mathbf{k}) + 1, \quad (31)$$

$$b_2(\mathbf{k}_1, \mathbf{k}_2) = b_2^L(\mathbf{k}_1, \mathbf{k}_2) - F_2(\mathbf{k}_1, \mathbf{k}_2)b_1^L(\mathbf{k}_{12}) + \{[\mathbf{k} \cdot \mathbf{L}_1(\mathbf{k}_1)]b_1^L(\mathbf{k}_2) + (\mathbf{k}_1 \leftrightarrow \mathbf{k}_2)\}, \quad (32)$$

$$b_3(\mathbf{k}_1, \mathbf{k}_2, \mathbf{k}_3) = b_3^L(\mathbf{k}_1, \mathbf{k}_2, \mathbf{k}_3) - [F_2(\mathbf{k}_1, \mathbf{k}_2)b_2^L(\mathbf{k}_{12}, \mathbf{k}_3) + \text{cyc.}] + [\mathbf{k} \cdot \mathbf{L}_1(\mathbf{k}_3)]b_2^L(\mathbf{k}_1, \mathbf{k}_2) + \text{cyc.}] + [F_2(\mathbf{k}_1, \mathbf{k}_2)F_2(\mathbf{k}_{12}, \mathbf{k}_3) + \text{cyc.}] - F_3(\mathbf{k}_1, \mathbf{k}_2, \mathbf{k}_3)]b_1^L(\mathbf{k}) - [\mathbf{k} \cdot \mathbf{L}_1(\mathbf{k}_3)F_2(\mathbf{k}_1, \mathbf{k}_2)b_1^L(\mathbf{k}_{12}) + \text{cyc.}] + \{[\mathbf{k} \cdot \mathbf{L}_2(\mathbf{k}_1, \mathbf{k}_2) + \mathbf{k} \cdot \mathbf{L}_1(\mathbf{k}_1)\mathbf{k} \cdot \mathbf{L}_1(\mathbf{k}_2) - \mathbf{k} \cdot \mathbf{L}_1(\mathbf{k}_{12})F_2(\mathbf{k}_1, \mathbf{k}_2)]b_1^L(\mathbf{k}_3) + \text{cyc.}\}, \quad (33)$$

and so forth, where $\mathbf{k} = \mathbf{k}_{1\dots n}$ for b_n .

An immediate consequence of the above formulas is that the biasing cannot be local simultaneously both in Eulerian and in Lagrangian space, since the bias parameters are all constants in local bias models. For example, when the Lagrangian bias is local and parameters b_1^L, b_2^L, \dots are scale-independent constants, the higher-order Eulerian parameters b_2, b_3, \dots are inevitably scale-dependent according to Eqs. (31)–(33). The reason for the incompatibility of local biases is that nonlinear evolutions are nonlocal process in general, as we already described in Introduction.

In spite of that, local relations between the Lagrangian halo bias and the local Eulerian bias parameters are known in the halo model [57]. These relations are derived by applying the spherical collapse model [53, 54], in which the density evolutions are local process, and therefore the local biases are compatible. This compatibility does not hold in generally non-spherical collapse [75].

D. Comments on the bias relations in the spherical collapse model

The purpose of this subsection is to find a relation between the bias parameters of general perturbation theory and that of spherical collapse model. As mentioned above, the spherical

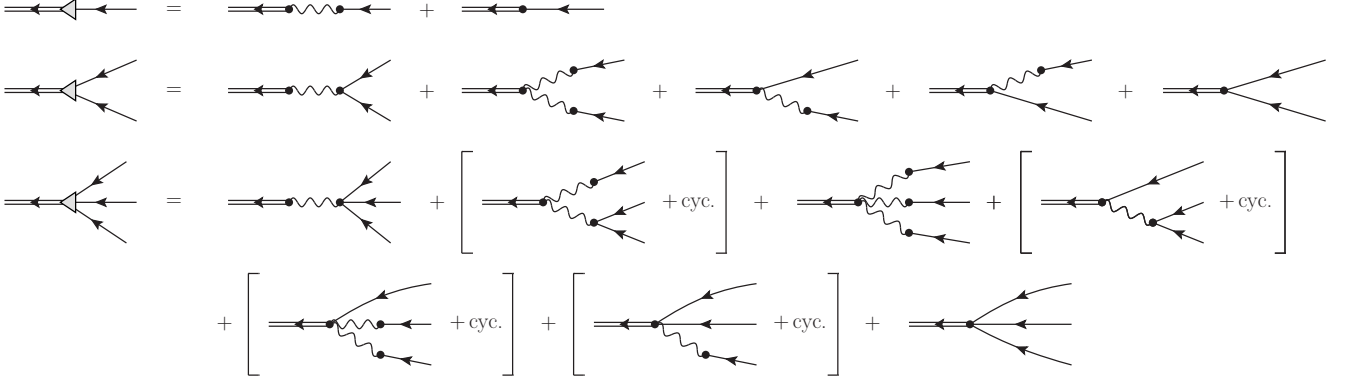


FIG. 8: Shrunken vertices in terms of the Lagrangian perturbation theory.

collapse model is used in the halo approach to find a local relation between the (Lagrangian) halo bias parameters and Eulerian bias parameters.

Following the same manner of Ref. [54], one can derive general relations between local bias parameters in Lagrangian space and in Eulerian space. Such relations are derived in Appendix A. Up to the third order, we have

$$b_1 = b_1^L + 1, \quad (34)$$

$$b_2 = b_2^L + \frac{8}{21}b_1^L, \quad (35)$$

$$b_3 = b_3^L - \frac{13}{7}b_2^L - \frac{796}{1323}b_1^L, \quad (36)$$

where both the Eulerian bias parameters $\{b_n\}$ and the Lagrangian bias parameters $\{b_n^L\}$ are local and scale-independent at the same time.

Remarkably, the local bias relations in Eqs. (34)–(36) for the spherical model can be derived from Eqs. (31)–(32) when the Lagrangian bias is local and Eulerian bias functions are averaged over directions of wavevectors. Each bias function $b_n^L(\mathbf{k}_1, \dots, \mathbf{k}_n)$ is replaced by a constant b_n^L in the local Lagrangian bias. Angular averages of Eqs. (31)–(33) in this case are straightforwardly calculated by using the explicit forms of F_2 , L_1 and L_2 in Eqs. (7), (23) and (24). The angular average of F_3 is given by $\langle F_3 \rangle = 682/189$ [20, 96]. As a result, the angular averages of Eqs. (31)–(33) exactly reduce to the right-hand sides of Eqs. (34)–(36).

Therefore, the scale- and angular-dependences of bias are neglected in the bias relations of the spherical collapse model, which are widely used in the halo approach. It is only when those dependences of bias are not important that the local bias relations of Eqs. (34)–(35) are useful. In general perturbations without spherical symmetry, one should use the nonlocal relations of bias in Eqs. (31)–(33).

E. Comments on the stochastic bias

In the framework of local bias models, the deterministic property of bias is not viable in reality. The number density of

observed objects is not solely determined by the local density of mass. The stochastic biasing scheme [69] is a phenomenological model to treat the biasing as a nondeterministic process, in the framework of local bias models.

One of the characteristic parameters of stochasticity is the correlation coefficient, defined by

$$r(R) = \frac{\langle \delta_m(R) \delta_X(R) \rangle}{\sigma_m(R) \sigma_X(R)}, \quad (37)$$

where $\sigma_m(R) = \langle \delta_m^2(R) \rangle^{1/2}$, $\sigma_X(R) = \langle \delta_X^2(R) \rangle^{1/2}$ are square roots of the variances of density contrasts $\delta_m(R)$, $\delta_X(R)$ which are smoothed by a radius R at a point in Eulerian space. If the deterministic relation $\delta_X(R) = b(R)\delta_m(R)$ exactly holds, the stochasticity parameter $r(R)$ is identically unity. Deviations of the stochasticity parameter from unity characterize how the stochasticity is important. It is also common to define the correlation coefficient in Fourier space,

$$r(k) = \frac{P_{mX}(k)}{\sqrt{P_m(k)P_X(k)}}, \quad (38)$$

where $P_{mX}(k)$ is the cross power spectrum of mass and objects, $P_m(k)$ and $P_X(k)$ are the power spectra of mass and objects, respectively.

This approach is purely phenomenological in the sense that the stochasticity itself does not correspond to any fundamental physics. Instead, the stochasticity represents our ignorance on the formation process of observed objects. Dynamical evolutions of density field and the formation process of observed objects are deterministic at the fundamental level. If we would know all the detailed physics of the formation process, any stochastic character should not appear when we properly describe precise dependences of the number density of objects on physical quantities, not only a local density of mass.

For the above reason, the parameters of stochastic bias should be derived from the nonlocal bias functions, $b_n(\mathbf{k}_1, \dots, \mathbf{k}_n)$. At linear order, the correlation coefficient in Fourier space $r(k)$ is identically unity, since the bias is multiplicative, $\delta_X(\mathbf{k}) = b_1(k)\delta_m(\mathbf{k})$, which is a consequence of the translational invariance. Even in this case, the correlation coefficient in configuration space, Eq. (37), is less than

unity in general when the linear bias parameter $b_1(k)$ is scale-dependent [63, 70].

At nonlinear orders, the correlation coefficient even in Fourier space becomes less than unity. It is straightforward to calculate the Eq. (38) in our framework of nonlocal biasing. The lowest-order contribution to $1 - r(k)$ is given by one-loop diagrams. The relevant diagrams are similar to Fig. 6, and the final result simply reduces to

$$1 - r(k) = \frac{1}{4[b_1(k)]^2 P_L(k)} \times \int \frac{d^3 k'}{(2\pi)^3} [b_2(\mathbf{k}', \mathbf{k} - \mathbf{k}')^2 P_L(k') P_L(|\mathbf{k} - \mathbf{k}'|)]. \quad (39)$$

This result is valid even when the initial density field is non-Gaussian. The bispectrum contributions to one-loop power spectra cancel out in the combination of Eq. (38).

In a case of local Lagrangian bias, including the halo bias, the Lagrangian functions b_n^L are constants and the second-order Eulerian bias function of Eq. (32) reduces to

$$b_2(\mathbf{k}_1, \mathbf{k}_2) = b_2^L + \frac{4}{7} \left[1 - \left(\frac{\mathbf{k}_1 \cdot \mathbf{k}_2}{k_1 k_2} \right)^2 \right] b_1^L. \quad (40)$$

In the large-scale limit, $k \rightarrow 0$, we have $b_2(\mathbf{k}', \mathbf{k} - \mathbf{k}') \rightarrow b_2^L$, and from Eq. (38),

$$1 - r(k) \rightarrow \frac{(b_2^L)^2}{4[b_1(k)]^2 P_L(k)} \int \frac{d^3 k'}{(2\pi)^3} [P_L(k')]^2. \quad (41)$$

It is interesting to note that the stochasticity emerges even in the large-scale limit when the second-order Lagrangian bias parameter b_2^L is nonzero. One cannot find such kind of properties in an original approach of the stochastic biasing, since the correlation coefficient is just a free parameter in the latter. The halo model actually predicts the nonzero value of the second-order bias parameter b_2^L (see Sec. V C below).

To summarize this subsection, the stochastic bias is a phenomenology which is conveniently introduced in the context of local bias models, and is not needed in nonlocal bias models. Stochastic properties of the local bias are derived from the deterministic nonlocal bias.

III. PERTURBATION THEORY IN REDSHIFT SPACE WITH NONLOCAL BIAS

A. Nonlocal bias in Eulerian space and redshift-space distortions

The comoving position \mathbf{x} in real space and s in redshift space are related by [71]

$$\mathbf{s} = \mathbf{x} + \frac{v_z(\mathbf{x})}{aH} \hat{\mathbf{z}}, \quad (42)$$

in the plane-parallel limit of the distant-observer approximation, where $\hat{\mathbf{z}}$ is the unit vector along the line of sight, and v_z is the velocity component along $\hat{\mathbf{z}}$. The number density field

in real space $\rho_X(\mathbf{x})$ and that in redshift space $\rho_X^s(s)$ are related by a continuity relation:

$$\rho_X^s(s) d^3 s = \rho_X(\mathbf{x}) d^3 x, \quad (43)$$

Therefore, the density contrast in redshift space is given by

$$\delta_X^s(s) = [1 + \delta_X(\mathbf{x})] J^{-1} - 1, \quad (44)$$

where $J = \partial(s)/\partial(\mathbf{x})$ is the Jacobian of the mapping from real space to redshift space. One can easily calculate the Fourier transform of Eq. (44):

$$\delta_X^s(\mathbf{k}) = \int d^3 x e^{-i\mathbf{k} \cdot \mathbf{x}} [1 + \delta_X(\mathbf{x})] e^{i\mathbf{k} \cdot \mathbf{u}_z(\mathbf{x})}, \quad (45)$$

where $\mathbf{u}_z = -v_z/aH$ and $\mathbf{k} \neq \mathbf{0}$ is assumed. A different expression of the above formula is seen in the Eq. (4) of Ref. [44], and it can be shown by partial integration that the two expressions are actually equivalent. The above relation is applicable even in the fully nonlinear regime.

In Fourier space,

$$u_z(\mathbf{k}) = -ik_z \theta(\mathbf{k})/k^2, \quad (46)$$

where $\theta(\mathbf{k})$ is the Fourier transform of the normalized velocity convergence, $\theta = -\nabla \cdot \mathbf{v}/aH$. Expanding the peculiar velocity field in Eq. (45), we have

$$\begin{aligned} \delta_X^s(\mathbf{k}) &= \sum_{n+m \geq 1} \frac{(\mu k)^n}{n!m!} \int \frac{d^3 k_1}{(2\pi)^3} \cdots \frac{d^3 k_n}{(2\pi)^3} \frac{d^3 k'_1}{(2\pi)^3} \cdots \frac{d^3 k'_m}{(2\pi)^3} \\ &\times (2\pi)^3 \delta_D^3(\mathbf{k}_{1\dots n} + \mathbf{k}'_{1\dots m} - \mathbf{k}) \frac{\mu_1 \cdots \mu_n}{k_1 \cdots k_n} b_m(\mathbf{k}'_1, \dots, \mathbf{k}'_m) \\ &\times \theta(\mathbf{k}_1) \cdots \theta(\mathbf{k}_n) \delta_m(\mathbf{k}'_1) \cdots \delta_m(\mathbf{k}'_m), \end{aligned} \quad (47)$$

where we define $b_0 \equiv 1$ above just for $m = 0$, and $\mu \equiv \mathbf{k} \cdot \hat{\mathbf{z}}/k$, $\mu_i \equiv \mathbf{k}_i \cdot \hat{\mathbf{z}}/k_i$ are direction cosines of wavevectors. It can be shown that this equation is equivalent to the Eq. (5) of Ref. [44], although the apparent expressions are somewhat different.

In the SPT, only growing-mode solutions in each order are retained, and the peculiar velocity field is consistently assumed to be irrotational. Thus, the velocity field is fully characterized by the velocity divergence [20], which is expanded by a linear density contrast as

$$\begin{aligned} \theta(\mathbf{k}) &= \sum_{n=1}^{\infty} \frac{f}{n!} \int \frac{d^3 k_1}{(2\pi)^3} \cdots \frac{d^3 k_n}{(2\pi)^3} (2\pi)^3 \delta_D^3(\mathbf{k}_{1\dots n} - \mathbf{k}) \\ &\times G_n(\mathbf{k}_1, \dots, \mathbf{k}_n) \delta_L(\mathbf{k}_1) \cdots \delta_L(\mathbf{k}_n), \end{aligned} \quad (48)$$

where $f = d \ln D / d \ln a = \dot{D}/HD$ is the linear growth rate which corresponds to the logarithmic derivative of the linear growth factor. The perturbative kernels G_n are given by SPT [15, 16, 18, 20]. For $n = 1, 2$, we have

$$G_1(\mathbf{k}) = 1, \quad (49)$$

$$G_2(\mathbf{k}_1, \mathbf{k}_2) = \frac{6}{7} + \left(\frac{k_1}{k_2} + \frac{k_2}{k_1} \right) \frac{\mathbf{k}_1 \cdot \mathbf{k}_2}{k_1 k_2} + \frac{8}{7} \left(\frac{\mathbf{k}_1 \cdot \mathbf{k}_2}{k_1 k_2} \right)^2, \quad (50)$$

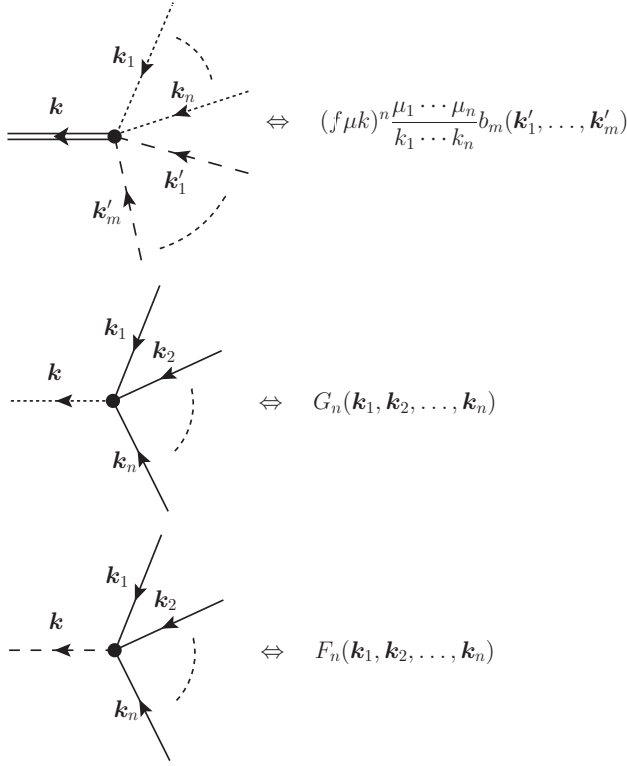


FIG. 9: Diagrammatic rules for the Eulerian perturbation theory in redshift space. In the first rule, $\mathbf{k} = \mathbf{k}_1 + \dots + \mathbf{k}_n + \mathbf{k}'_1 + \dots + \mathbf{k}'_m$ should be satisfied, and $\mathbf{k} = \mathbf{k}_1 + \dots + \mathbf{k}_n$ should be satisfied in the last two rules. The dashed lines and dotted lines are internal.

where the expression G_2 is exact only in Einstein–de-Sitter universe, and only weakly depends on time in general cosmology.

Fig. 9 shows the diagrammatic rules for the Eulerian perturbation theory in redshift space. The first rule corresponds to the expansion of Eq. (47), and the second rule corresponds to Eq. (48). The rules are used in a similar way of those in real space. The third rule is common to the rule in real space, and corresponds to Eq. (5). The momentum conservation should be satisfied in each vertex. The meanings of double solid line, dashed line and single solid line are the same as in real space. The dotted line corresponds to the velocity convergence θ .

Substituting the perturbative expansions of Eqs. (5) and (48) into Eq. (47), we have a formal series of the biased field in redshift space:

$$\delta_X^s(\mathbf{k}) = \sum_{n=1}^{\infty} \int \frac{d^3 k_1}{(2\pi)^3} \dots \frac{d^3 k_n}{(2\pi)^3} (2\pi)^3 \delta^3(\mathbf{k}_{1\dots n} - \mathbf{k}) \times S_n(\mathbf{k}_1, \dots, \mathbf{k}_n) \delta_L(\mathbf{k}_1) \dots \delta_L(\mathbf{k}_n), \quad (51)$$

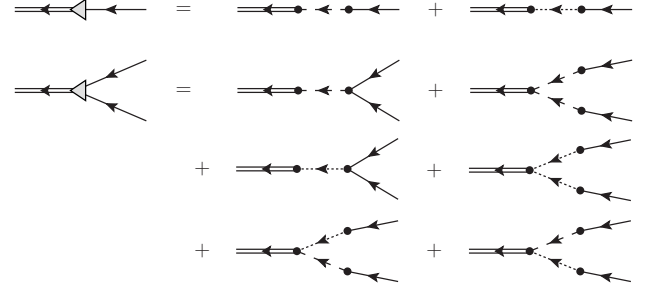


FIG. 10: Shrunk vertices in Eulerian perturbation theory in redshift space.

where S_n 's are derived kernels. For $n = 1, 2$, we have

$$S_1(\mathbf{k}) = b_1(\mathbf{k}) + f\mu^2, \quad (52)$$

$$S_2(\mathbf{k}_1, \mathbf{k}_2) = b_1(\mathbf{k}_{12})F_2(\mathbf{k}_1, \mathbf{k}_2) + b_2(\mathbf{k}_1, \mathbf{k}_2) + f\mu^2 G_2(\mathbf{k}_1, \mathbf{k}_2) + (f\mu k)^2 \frac{\mu_1 \mu_2}{k_1 k_2} + f\mu k \left[\frac{\mu_1}{k_1} b_1(\mathbf{k}_2) + \frac{\mu_2}{k_2} b_1(\mathbf{k}_1) \right]. \quad (53)$$

In the case of local biasing where b_1 and b_2 are constants, these kernels are equivalent to the Eqs. (11) and (12) in Ref. [44]. Those equations are diagrammatically represented in Fig. 10.

B. Nonlocal bias in Lagrangian space and redshift-space distortions

Redshift-space distortions are naturally derived in the Lagrangian picture. The velocity of a mass element with Lagrangian coordinates \mathbf{q} is given by a simple derivative of Eq. (15):

$$\mathbf{v}(\mathbf{q}) = a\dot{\mathbf{x}}(\mathbf{q}) = a\dot{\Psi}(\mathbf{q}), \quad (54)$$

where the dot represents a partial derivative by the proper time t . Note that we suppress the argument of the time t in our variables. From Eq. (42), the displacement field in redshift space is simply given by

$$\Psi^s = \Psi + \frac{\hat{\mathbf{z}} \cdot \dot{\Psi}}{H} \hat{\mathbf{z}}. \quad (55)$$

The redshift-space distortions are exactly linear mappings of the displacement field, even in the nonlinear regime [39]. A similar equation has been applied to the analysis of the Zel'dovich approximation [72].

In our approximation that the perturbative kernels L_n are independent on time, we have $\Psi^{(n)} \propto D^n$, where $\Psi^{(n)}$ is the configuration-space counterpart of n -th order term in Eq.(22). Therefore, the time derivative of the displacement field is simply given by

$$\dot{\Psi}^{(n)} = nHf\Psi^{(n)}, \quad (56)$$

and the displacement field of each order in redshift space is related to the real-space displacement via

$$\boldsymbol{\Psi}^{s(n)} = \boldsymbol{\Psi}^{(n)} + nf(\hat{\mathbf{z}} \cdot \boldsymbol{\Psi}^{(n)}) \hat{\mathbf{z}}, \quad (57)$$

which is just a linear mapping of the displacement field in each order. This linear transformation is characterized by a redshift-space distortion tensor $R_{ij}^{(n)}$ for each n [39], which is defined by

$$R_{ij}^{(n)} = \delta_{ij} + nf\hat{z}_i\hat{z}_j. \quad (58)$$

The Eq. (57) reduces to $\Psi_i^{s(n)} = R_{ij}^{(n)}\Psi_j^{(n)}$, or in a vector notation, $\boldsymbol{\Psi}^{s(n)} = R^{(n)}\boldsymbol{\Psi}^{(n)}$.

As a result, each perturbative kernel of the redshift-space displacement is given by a linear transformation from the real-space kernel,

$$\mathbf{L}_n^s = R^{(n)}\mathbf{L}_n. \quad (59)$$

For $n = 1, 2$, we have

$$\mathbf{L}_1^s(\mathbf{k}) = \frac{\mathbf{k} + f\mu k\hat{\mathbf{z}}}{k^2}, \quad (60)$$

$$\mathbf{L}_2^s(\mathbf{k}_1, \mathbf{k}_2) = \frac{3}{7} \frac{\mathbf{k} + 2f\mu k\hat{\mathbf{z}}}{k^2} \left[1 - \left(\frac{\mathbf{k}_1 \cdot \mathbf{k}_2}{k_1 k_2} \right)^2 \right], \quad (61)$$

where $\mathbf{k} = \mathbf{k}_1 + \mathbf{k}_2$ for \mathbf{L}_2^s . All the formalism of Sec. II B in real space applies with substitutions of $\mathbf{L}_n \rightarrow \mathbf{L}_n^s$ and $K_n \rightarrow S_n$ in redshift space. Corresponding to Eqs. (25) and (26), we have

$$S_1(\mathbf{k}) = \mathbf{k} \cdot \mathbf{L}_1^s(\mathbf{k}) + b_1^L(\mathbf{k}), \quad (62)$$

$$\begin{aligned} S_2(\mathbf{k}_1, \mathbf{k}_2) &= \mathbf{k} \cdot \mathbf{L}_2^s(\mathbf{k}_1, \mathbf{k}_2) + [\mathbf{k} \cdot \mathbf{L}_1^s(\mathbf{k}_1)][\mathbf{k} \cdot \mathbf{L}_1^s(\mathbf{k}_2)] \\ &\quad + b_1^L(\mathbf{k}_1)[\mathbf{k} \cdot \mathbf{L}_1^s(\mathbf{k}_2)] + b_1^L(\mathbf{k}_2)[\mathbf{k} \cdot \mathbf{L}_1^s(\mathbf{k}_1)] \\ &\quad + b_2^L(\mathbf{k}_1, \mathbf{k}_2), \end{aligned} \quad (63)$$

and so forth, where $\mathbf{k} = \mathbf{k}_{1\dots n}$ for S_n . Substituting Eqs. (60), (61), and Eqs. (31), (32), the above equations are equivalent to Eqs. (52), (53). Thus, the relation of the nonlocal biases of Eqs. (31), (32), which are derived in real space, also consistently applies in redshift space. Such consistency should hold for any higher-order kernels.

IV. VERTEX RESUMMATIONS

The formalism presented so far is a natural extension of the SPT, simultaneously including the nonlocal bias, redshift-space distortions and primordial non-Gaussianity. In recent years, various methods beyond the SPT are developed as mentioned in Introduction. In the RPT [31, 32], the ‘‘propagator’’ plays an important role. The concept of the propagator is extended to the ‘‘multi-point propagator’’ [73, 74], in which the original propagator is identified as the one-point propagator.

In this section, we show that the multi-point propagators can be obtained by resumming the external vertices in our formalism. Most of the resummation methods known so far are

only applied to the dark matter clustering in real space. Exceptions are the Lagrangian resummation method [39, 75], in which local Lagrangian bias and redshift-space distortions are included, and the time-renormalization-group method [76]), in which the halo bias is included. Therefore, the identification of the multi-point propagators in our formalism is an important step toward including all the effects of nonlocal biasing, redshift-space distortions and primordial non-Gaussianity into the resummation methods.

A. Multi-point propagators

We first consider how the multi-point propagator [73] is related to our formalism. We only consider one-component propagators with the density sector. The n -th order propagator $\Gamma_m^{(n)}(\mathbf{k}_1, \dots, \mathbf{k}_n)$ of the density sector is defined by an ensemble average of the functional derivative:

$$\left\langle \frac{\delta^n \delta_m(\mathbf{k})}{\delta \delta_L(\mathbf{k}_1) \cdots \delta \delta_L(\mathbf{k}_n)} \right\rangle = (2\pi)^{3-3n} \delta_D^3(\mathbf{k} - \mathbf{k}_{1\dots n}) \Gamma_m^{(n)}(\mathbf{k}_1, \dots, \mathbf{k}_n). \quad (64)$$

The original multi-point propagator $\Gamma_{ab_1\dots b_n}^{(n)}$ with density and velocity sectors, defined in Refs. [73, 74], is related to our definition of density propagator by $\Gamma_m^{(n)} = n!2^{-n}(D_{\text{init}}/D)^n \Gamma_{1a_1\dots a_n}^{(n)} u_{a_1} \cdots u_{a_n}$, where D_{init} is the linear growth factor at the initial time t_{init} . The appearance of the Dirac’s delta function on the right-hand side of Eq. (64) is due to the translational symmetry. When the initial density field is random Gaussian, the multi-point propagator of Eq. (64) corresponds to the coefficient of orthogonal expansion by a series of generalized Wiener-Hermite functionals [77].

Substituting Eq. (5) into the left-hand side of Eq. (64), we have

$$\begin{aligned} \left\langle \frac{\delta^n \delta_m(\mathbf{k})}{\delta \delta_L(\mathbf{k}_1) \cdots \delta \delta_L(\mathbf{k}_n)} \right\rangle &= \frac{1}{(2\pi)^{3n}} \sum_{m=0}^{\infty} \frac{1}{m!} \int \frac{d^3 k'_1}{(2\pi)^3} \cdots \frac{d^3 k'_m}{(2\pi)^3} \\ &\quad \times (2\pi)^3 \delta_D^3(\mathbf{k} - \mathbf{k}_{1\dots n} - \mathbf{k}'_{1\dots m}) F_{n+m}(\mathbf{k}_1, \dots, \mathbf{k}_n, \mathbf{k}'_1, \dots, \mathbf{k}'_m) \\ &\quad \times \langle \delta_L(\mathbf{k}'_1) \cdots \delta_L(\mathbf{k}'_m) \rangle. \end{aligned} \quad (65)$$

The last factor is proportional to $\delta_D^3(\mathbf{k}'_{1\dots m})$ for the translational symmetry, and the remaining factor is further decomposed into products of connected polyspectra, $\sum \prod P^{(N)}$. For example,

$$\begin{aligned} \langle \delta_1 \delta_2 \delta_3 \delta_4 \rangle &= \langle \delta_1 \delta_2 \delta_3 \delta_4 \rangle_c + \langle \delta_1 \delta_2 \rangle_c \langle \delta_3 \delta_4 \rangle_c \\ &\quad + \langle \delta_1 \delta_3 \rangle_c \langle \delta_2 \delta_4 \rangle_c + \langle \delta_1 \delta_4 \rangle_c \langle \delta_2 \delta_3 \rangle_c \\ &= \delta_{1234}^D P_{1234}^{(4)} + \delta_{12}^D \delta_{34}^D P_{12}^{(2)} P_{34}^{(2)} \\ &\quad + \delta_{13}^D \delta_{24}^D P_{13}^{(2)} P_{24}^{(2)} + \delta_{14}^D \delta_{23}^D P_{14}^{(2)} P_{23}^{(2)}, \end{aligned} \quad (66)$$

and so forth, where $\delta_1 = \delta(\mathbf{k}'_1)$, $\delta_2 = \delta(\mathbf{k}'_2)$, $\delta_{1234}^D = (2\pi)^3 \delta_D^3(\mathbf{k}'_{1234})$, $P_{1234}^{(4)} = P(\mathbf{k}'_1, \dots, \mathbf{k}'_4)$, etc. Thus we have

$$\begin{aligned} \Gamma_m^{(n)}(\mathbf{k}_1, \dots, \mathbf{k}_n) &= \sum_{m=0}^{\infty} \frac{1}{m!} \int \frac{d^3 k'_1}{(2\pi)^3} \cdots \frac{d^3 k'_m}{(2\pi)^3} \\ &\quad \times F_{n+m}(\mathbf{k}_1, \dots, \mathbf{k}_n, \mathbf{k}'_1, \dots, \mathbf{k}'_m) \langle \delta_L(\mathbf{k}'_1) \cdots \delta_L(\mathbf{k}'_m) \rangle. \end{aligned} \quad (67)$$

This equation is equivalent to Eq. (23) of Ref. [74] when the last term is decomposed into connected parts. The graphical representation of Eq. (67) is similar to Fig. 2 of Ref. [73].

Let us extend the above multi-point propagator of mass density field to include the effects of biasing and redshift-space distortions. We define the n -th order propagator $\Gamma_X^{(n)}(\mathbf{k}_1, \dots, \mathbf{k}_n)$ of the objects X by

$$\left\langle \frac{\delta^n \delta_X(\mathbf{k})}{\delta \delta_L(\mathbf{k}_1) \cdots \delta \delta_L(\mathbf{k}_n)} \right\rangle = (2\pi)^{3-3n} \delta_D^3(\mathbf{k} - \mathbf{k}_{1\dots n}) \Gamma_X^{(n)}(\mathbf{k}_1, \dots, \mathbf{k}_n). \quad (68)$$

Substituting Eq. (8) into the above equation, and following the same way of obtaining the Eq. (67), we have

$$\Gamma_X^{(n)}(\mathbf{k}_1, \dots, \mathbf{k}_n) = \sum_{m=0}^{\infty} \frac{1}{m!} \int \frac{d^3 k'_1}{(2\pi)^3} \cdots \frac{d^3 k'_m}{(2\pi)^3} \times K_{n+m}(\mathbf{k}_1, \dots, \mathbf{k}_n, \mathbf{k}'_1, \dots, \mathbf{k}'_m) \langle \delta_L(\mathbf{k}'_1) \cdots \delta_L(\mathbf{k}'_m) \rangle. \quad (69)$$

To include the redshift-space distortions, one simply apply the substitution $K_{n+m} \rightarrow S_{n+m}$ in the above equation. The diagrammatic representation of this equation is given in Fig. 11.

The usage of the multi-point propagator is parallel to the one in Refs. [73, 74]. The multi-point propagator corresponds to the summation of all the loops which are attached to each external vertex. Therefore, the polyspectra $P_X^{(N)}$ of Eq. (12) are represented by using the multi-point propagators and corresponding diagrams do not have any loop which is attached to a single external vertex of the multi-point propagator. For example, Fig. 12 represents the power spectrum of the object for the Gaussian initial conditions. The resulting power spectrum is given by

$$P_X(k) = \sum_{n=0}^{\infty} \frac{1}{n!} \int \frac{d^3 k_1}{(2\pi)^3} \cdots \frac{d^3 k_n}{(2\pi)^3} (2\pi)^3 \delta_D^3(\mathbf{k} - \mathbf{k}_{1\dots n}) \times \left| \Gamma_X^{(n)}(\mathbf{k}_1, \dots, \mathbf{k}_n) \right|^2 P_L(k_1) \cdots P_L(k_n). \quad (70)$$

As described in Ref. [73], it is important to note that each term in the sum is positive and the subsequent contributions add constructively.

B. Lagrangian vertex resummations

The multi-point propagators are still difficult to be exactly evaluated. One of the remarkable results in the RPT is a derivation of the propagators in the high- k limit [31, 32, 73, 74]. It is not trivial whether or not the same limit can be calculated in the presence of bias. Investigations on this line will be interesting for future work, and we leave them as an open question. Instead of evaluating the full expression of the multi-point propagators, we consider partial resummations of external vertex in the Lagrangian representation of the perturbation theory in this section.

As obviously seen in Fig. 11, the multi-point propagator is essentially a renormalized external vertex. First we consider

partial resummation of the external vertex given in Fig. 13. In this figure, the gray ellipse represents all the possible graphs which are attached to a single external vertex with r wavy lines. The graphs in the gray ellipse are not necessarily connected, and can be disconnected as illustrated in the second line of the figure.

According to the diagrammatic rules of Fig. 7 and appropriate statistical factors, the corresponding factor of Fig. 13 reduces to

$$\begin{aligned} & \sum_{r=0}^{\infty} \frac{(-i)^r}{r!} \int \frac{d^3 k'_1}{(2\pi)^3} \cdots \frac{d^3 k'_r}{(2\pi)^3} \langle [\tilde{\Psi}_{j_1}(\mathbf{k}'_1)] \cdots [\tilde{\Psi}_{j_r}(\mathbf{k}'_r)] \rangle \\ & \quad \times b_n^L(\mathbf{k}_1, \dots, \mathbf{k}_n) k_{i_1} \cdots k_{i_m} k_{j_1} \cdots k_{j_r} \\ & = \sum_{r=0}^{\infty} \frac{(-i)^r}{r!} \left\langle \left[\int \frac{d^3 k'}{(2\pi)^3} \mathbf{k} \cdot \tilde{\Psi}(\mathbf{k}') \right]^r \right\rangle b_n^L(\mathbf{k}_1, \dots, \mathbf{k}_n) k_{i_1} \cdots k_{i_m} \\ & = \langle e^{-i\mathbf{k} \cdot \Psi} \rangle b_n^L(\mathbf{k}_1, \dots, \mathbf{k}_n) k_{i_1} \cdots k_{i_m}, \end{aligned} \quad (71)$$

where

$$\Psi = \Psi(\mathbf{0}) = \int \frac{d^3 k'}{(2\pi)^3} \tilde{\Psi}(\mathbf{k}'), \quad (72)$$

is the displacement vector at the origin. The factor

$$\Pi(\mathbf{k}) \equiv \langle e^{-i\mathbf{k} \cdot \Psi} \rangle = \int d^3 \Psi e^{-i\mathbf{k} \cdot \Psi} \mathcal{P}(\Psi), \quad (73)$$

is the characteristic function of the one-point distribution of the displacement field, where $\mathcal{P}(\Psi)$ is the one-point probability function of the displacement field. This characteristic function is a generating function of moments of Ψ at a single point in configuration space:

$$\langle \Psi_{j_1} \cdots \Psi_{j_n} \rangle = \frac{i^n \partial^n \Pi(\mathbf{k})}{\partial k_{j_1} \cdots \partial k_{j_n}} \Big|_{\mathbf{k}=\mathbf{0}}. \quad (74)$$

The characteristic function is represented by a connected moments by the cumulant expansion theorem [78]:

$$\begin{aligned} \Pi(\mathbf{k}) &= \exp \left[\sum_{n=1}^{\infty} \frac{(-i)^n}{n!} \langle (\mathbf{k} \cdot \Psi)^n \rangle_c \right] \\ &= \exp \left[\sum_{n=1}^{\infty} \frac{(-i)^n}{n!} k_{j_1} \cdots k_{j_n} \langle \Psi_{j_1} \cdots \Psi_{j_n} \rangle_c \right]. \end{aligned} \quad (75)$$

In real space, the cumulants of the last line of the above equation are nonzero only when n is an even number for the rotational symmetry, and have the form

$$\langle \Psi_{j_1} \cdots \Psi_{j_n} \rangle_c = A_{2n} \frac{2^n n!}{(2n)!} (\delta_{j_1 j_2} \delta_{j_3 j_4} \cdots \delta_{j_{2n-1} j_{2n}} + \text{perm.}), \quad (76)$$

where the factor $(2n)!/2^n n!$ is the number of all the possible pairings among indices j_1, \dots, j_{2n} , and equals to the number of terms in the parenthesis. When all j_1, \dots, j_{2n} take the same component, e.g., z -axis, we have

$$\begin{aligned} \langle (\Psi_z)^{2n} \rangle &= \langle |\Psi|^{2n} (\cos \theta)^{2n} \rangle_c = \langle |\Psi|^{2n} \rangle_c \langle (\cos \theta)^{2n} \rangle \\ &= \frac{\langle |\Psi|^{2n} \rangle_c}{2n+1}, \end{aligned} \quad (77)$$

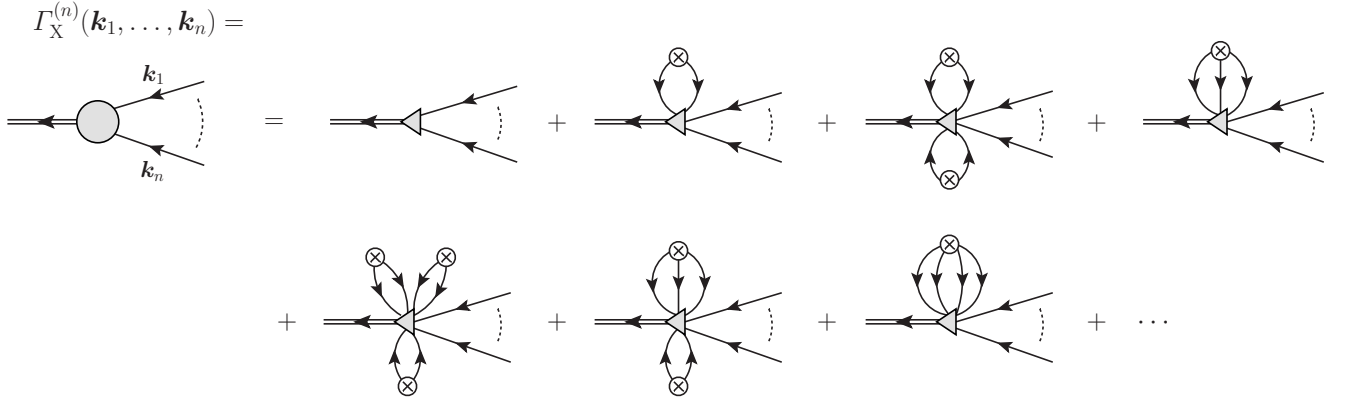


FIG. 11: Diagrammatic representation of the multi-point propagator of objects in real/redshift space.

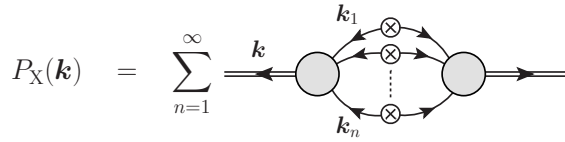


FIG. 12: Diagrammatic representation of the power spectrum with multi-point propagators when the initial density field is Gaussian. Effects of biasing and redshift-space distortions are included in the multi-point propagators in our formalism.

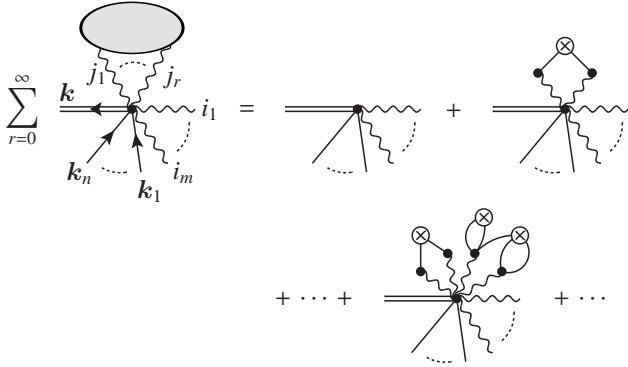


FIG. 13: Vertex resummation with displacement legs.

where θ is the polar angle of Ψ , and we used the fact that the variables $|\Psi|$ and θ are independent and the directional cosine is randomly distributed in real space.

Comparing Eqs. (76) and (77), we have

$$A_{2n} = \frac{\langle |\Psi|^{2n} \rangle_c}{2n+1}. \quad (78)$$

This equation can also be directly confirmed by contracting

Eq. (76) for each n . Thus Eq. (75) reduces to

$$\Pi(k) = \exp \left[\sum_{n=1}^{\infty} \frac{(-1)^n A_{2n} k^{2n}}{(2n)!} \right] = \exp \left[\sum_{n=1}^{\infty} \frac{(-1)^n \langle |\Psi|^{2n} \rangle_c}{(2n+1)(2n)!} k^{2n} \right]. \quad (79)$$

When the higher-order cumulants of displacement field are negligible on large scales, the above equation reduces to a Gaussian damping factor,

$$\Pi(k) \simeq \exp \left(-\frac{k^2}{6} \langle |\Psi|^2 \rangle \right). \quad (80)$$

Therefore the large-scale power spectrum is smeared by non-linear effects, and such smearing is important in the analysis of BAO [39, 79].

The above Eq. (79), however, is valid only in real space where the clustering is statistically isotropic. In redshift space, the clustering is not statistically isotropic and Eq. (75) should be evaluated with the displacement field Ψ^s of Eq. (55). When the lowest-order (Zel'dovich) approximation is valid on large scales, and higher-order cumulants of the displacement field is negligible (i.e., primordial non-Gaussianity is weak), we have again a Gaussian damping factor,

$$\Pi(k) \simeq \exp \left\{ -\frac{k^2}{6} \left[1 + f(f+2)\mu^2 \right] \langle |\Psi|^2 \rangle \right\}, \quad (81)$$

where $\mu = k_z/k$ is the direction cosine of the wavevector with respect to the lines of sight. This damping factor represents both effects of nonlinear smearing and FoG in redshift space [39], which are present even on large scales. The damping factor of FoG is similar to, but somewhat different from that adopted in a phenomenological modeling [47–49], $\exp(-f^2 \mu^2 k^2 \sigma_v^2 / 2)$, where σ_v^2 is equal to $\langle |\Psi|^2 \rangle / 3$ at the linear order.

Next we consider partial resummation of the external vertex given in Fig. 14. As in Fig. 13, the gray ellipse represents all the possible graphs which are attached to a single external vertex with r solid lines. The graphs in the ellipse are not necessarily connected. The corresponding factor of Fig. 14

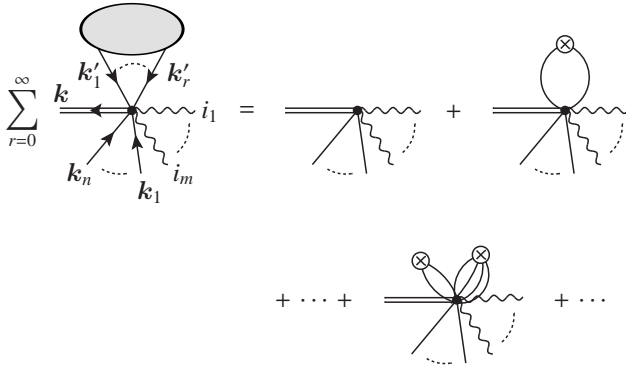


FIG. 14: Vertex resummation with bias legs.

reduces to

$$\begin{aligned}
 & \sum_{r=0}^{\infty} \frac{1}{r!} \int \frac{d^3 k'_1}{(2\pi)^3} \cdots \frac{d^3 k'_r}{(2\pi)^3} b_{n+r}^L(\mathbf{k}_1, \dots, \mathbf{k}_n, \mathbf{k}'_1, \dots, \mathbf{k}'_r) \\
 & \quad \times \langle \delta_L(\mathbf{k}'_1) \cdots \delta_L(\mathbf{k}'_r) \rangle k_{i_1} \cdots k_{i_m} \\
 & = (2\pi)^{3n} \int \frac{d^3 k'}{(2\pi)^3} \left\langle \frac{\delta^n \delta_X^L(\mathbf{k}')}{\delta \delta_L(\mathbf{k}_1) \cdots \delta \delta_L(\mathbf{k}_n)} \right\rangle k_{i_1} \cdots k_{i_m} \\
 & = c_n^L(\mathbf{k}_1, \dots, \mathbf{k}_n) k_{i_1} \cdots k_{i_m}, \tag{82}
 \end{aligned}$$

where we define the renormalized nonlocal bias function in Lagrangian space:

$$c_n^L(\mathbf{k}_1, \dots, \mathbf{k}_n) = (2\pi)^{3n} \int \frac{d^3 k'}{(2\pi)^3} \left\langle \frac{\delta^n \delta_X^L(\mathbf{k}')}{\delta \delta_L(\mathbf{k}_1) \cdots \delta \delta_L(\mathbf{k}_n)} \right\rangle. \tag{83}$$

This expression is contrasted with Eq. (20). Instead of evaluating the functional derivatives at $\delta_L = 0$, taking statistical averages of them gives the renormalized bias functions.

While the original function b_n^L can be determined solely by a functional relation between biased field and linear density field in Lagrangian space, the renormalized function c_n^L depends on the statistical properties of the linear (initial) density field. In configuration space, Eq. (83) is equivalent to

$$c_n^L(\mathbf{q} - \mathbf{q}_1, \dots, \mathbf{q} - \mathbf{q}_n) = \left\langle \frac{\delta^n \delta_X^L(\mathbf{q})}{\delta \delta_L(\mathbf{q}_1) \cdots \delta \delta_L(\mathbf{q}_n)} \right\rangle, \tag{84}$$

where the translational invariance is taken into account. We use the same symbols for variables both in Fourier space and configuration space as long as the notation is obvious. When a model of the Lagrangian bias is provided in configuration space, the renormalized bias functions are evaluated by the above equation.

Taylor expansions are possible only when the number density field δ_X^L is a smooth functional of the linear density field δ_L . However, the renormalized bias function c_n^L can be evaluated even when the biased field δ_X^L is not a smooth functional of δ_L and does not have a Taylor expansion, since statistical average in Eq. (83) is possible even when the functional derivative in the bracket is a singular functional. We will see

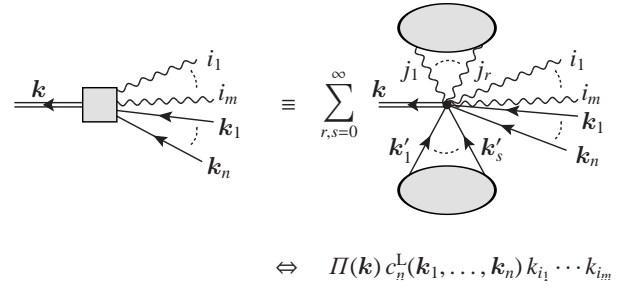


FIG. 15: Partial resummation of the vertex.

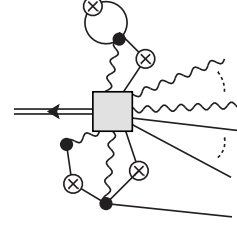


FIG. 16: An example of graphs that are not resummed in Eq. (85) or Fig. 15.

some examples below in which the bias cannot be expanded by a Taylor series while the renormalized bias functions are still well-defined.

Putting the diagrams of Fig. 13 and Fig. 14 together, we define the partial resummation of the external vertex in Fig. 15. The gray box in this figure represents the partial resummation with all the sub-graphs which are attached to an external vertex with only wavy lines and with only solid lines. The partial resummation of Fig. 15 results in the factor

$$\Pi(\mathbf{k}) c_n^L(\mathbf{k}_1, \dots, \mathbf{k}_n) k_{i_1} \cdots k_{i_m}. \tag{85}$$

Connected graphs with both wavy and solid lines attached to an external vertex are missed in this resummation. For example, graphs like Fig. 16 are not included in the factor of Eq. (85). To obtain the full multi-point propagators, all kinds of graphs like the one in Fig. 16 should be added. For example, the first-order propagator $\Gamma_X^{(2)}$ is diagrammatically given by Fig. 17 up to one-loop contributions.

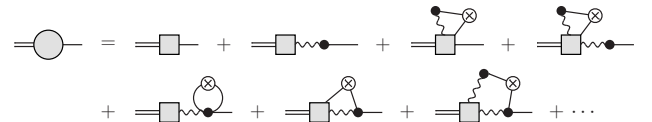


FIG. 17: First-order propagator with partially resummed vertex up to one-loop contributions.

V. SOME MODELS OF THE LAGRANGIAN BIAS

A. Local Lagrangian bias

In the case of the local Lagrangian bias, the linear density field in Lagrangian space, $\delta_X^L(\mathbf{q})$ is given by a single function of the smoothed mass density field $\delta_R(\mathbf{q})$ at the same position, where R is a smoothing radius. In configuration space, we have

$$\delta_X^L = F_X(\delta_R), \quad (86)$$

where F_X is generally a nonlinear, univariate function, and the smoothed mass density field in Lagrangian space is given by

$$\delta_R(\mathbf{q}) = \int d^3q' W_R(|\mathbf{q} - \mathbf{q}'|) \delta_L(\mathbf{q}'), \quad (87)$$

where the window function W_R is spherically symmetric. Applying the Taylor expansion and the Fourier transform to Eq. (86), the Lagrangian bias functions b_n^L in Eq. (20) reduces to

$$b_n^L(\mathbf{k}_1, \dots, \mathbf{k}_n) = F_X^{(n)}(0) W(k_1 R) \cdots W(k_n R), \quad (88)$$

where $F_X^{(n)} = d^n F_X / d\delta_R^n$ is the n -th derivative of the function F_X , and $W(kR)$ is a (3-dimensional) Fourier transform of the smoothing window function $W_R(x)$. The renormalized bias function c_n^L of Eq. (83) reduces to

$$c_n^L(\mathbf{k}_1, \dots, \mathbf{k}_n) = \langle F_X^{(n)}(\delta_R) \rangle W(k_1 R) \cdots W(k_n R). \quad (89)$$

By denoting $\mathcal{P}(\delta_R)$ as the probability distribution function of δ_R , the first factor of the above equation is given by

$$\begin{aligned} \langle F_X^{(n)}(\delta_R) \rangle &= \int_{-\infty}^{\infty} d\delta_R \mathcal{P}(\delta_R) F_X^{(n)}(\delta_R) \\ &= (-1)^n \int_{-\infty}^{\infty} d\delta_R \mathcal{P}^{(n)}(\delta_R) F_X(\delta_R), \end{aligned} \quad (90)$$

where $\mathcal{P}^{(n)} = d^n \mathcal{P} / d\delta_R^n$.

On scales which are larger than the smoothing scale, $|\mathbf{k}_i| < 1/R$ ($i = 1, \dots, n$), one can ignore the window function $W(kR)$ in Eqs. (88) and (89). In this case the Lagrangian bias functions are constants:

$$b_n^L(\mathbf{k}_1, \dots, \mathbf{k}_n) \simeq F_X^{(n)}(0), \quad (91)$$

$$c_n^L(\mathbf{k}_1, \dots, \mathbf{k}_n) \simeq \langle F_X^{(n)} \rangle. \quad (92)$$

One notices that Eq. (88) is well-defined only when the bias function F_X is a smooth function, because the factor $F_X^{(n)}(0)$ corresponds to a coefficient of the Taylor series. However, Eq. (89) is applicable even when the bias function is not a smooth function. As an illustration, we consider a threshold bias given by

$$F_X(\delta_R) = C \Theta(\delta_R - \delta_t) - 1, \quad (93)$$

where a constant δ_t is a threshold value,

$$C = \langle \Theta(\delta_R - \delta_t) \rangle^{-1} = \left[\int_{\delta_t}^{\infty} d\delta_R \mathcal{P}(\delta_R) \right]^{-1}, \quad (94)$$

and Θ is the step function. The Taylor expansion of this function is not well-defined since all the derivatives at the origin are zero, $F_X^{(n)}(0) = 0$ ($n \geq 1$), and we have $b_n^L = 0$ from Eq. (88). However, the expectation value in Eq. (89) is not zero in this case, and using Eq. (90) we have

$$\langle F_X^{(n)}(\delta_R) \rangle = (-1)^n C \int_{\delta_t}^{\infty} d\delta_R \mathcal{P}^{(n)}(\delta_R), \quad (95)$$

for $n \geq 1$. Therefore, the concept of renormalized bias functions c_n^L extends the applicability to the case when the simple Taylor expansion of the bias in Eq. (19) does not work.

In the limit $\delta_t \rightarrow \infty$, the threshold bias can be considered as an approximation to the peaks bias in the high-peak limit. Lagrangian statistics in this limit have been widely studied in 1980's [58, 80–82]. The methods developed in those studies are essentially equivalent to applying the renormalized bias in this work to the case of local Lagrangian bias. The use of the partially resummed vertex of Eq. (85) in calculating loop-corrections to the power spectrum is equivalent to applying a recent formalism developed in Ref. [75] in a case of local Lagrangian biasing and Gaussian initial conditions. The present formalism is applicable even in cases of nonlocal Lagrangian biasing with primordial non-Gaussianity.

B. Multivariate Lagrangian bias

In a local bias model, the number density field δ_X^L is a function of the single variable δ_R of Eq. (87). We next consider the case in which the number density field is a multivariate function of variables which are convolutions of the linear density field. The multiple variables χ_α , ($\alpha = 1, 2, \dots$) in Lagrangian space are given by

$$\chi_\alpha(\mathbf{q}) = \int d^3q' U_\alpha(\mathbf{q} - \mathbf{q}') \delta_L(\mathbf{q}'), \quad (96)$$

where U_α 's are the convolution kernels. For example, if one of the variables χ_α is the linear gravitational potential Φ_L in Lagrangian space, the corresponding convolution kernel is given by $U = -G a^2 \bar{\rho}_m / |\mathbf{q} - \mathbf{q}'|$. If one of the variables is a derivative of a smoothed density field, say $\partial \delta_R(\mathbf{q}) / \partial q_i$, the kernel is $U = \partial W_R(|\mathbf{q} - \mathbf{q}'|) / \partial q_i$, and so forth.

The peaks bias is described by a function of the smoothed density field and its derivatives up to second order, $(\delta_R, \partial_i \delta_R, \partial_i \partial_j \delta_R)$ [60]. A multivariate bias model with two variables, δ_R and Φ_L , is recently considered in the context of scale-dependent halo bias with primordial non-Gaussianity [83–85]. A multivariate Eulerian bias model is also proposed [86].

In general, we consider the biased field $\delta_X^L(\mathbf{q})$ is a local function of a finite number of the variables $\chi_\alpha(\mathbf{q})$ at the same Lagrangian position. In configuration space, we have

$$\delta_X^L = F_X(\chi_1, \chi_2, \dots). \quad (97)$$

In this case, the Lagrangian bias function of Eq. (19) reduces

to

$$b_n^L(\mathbf{k}_1, \dots, \mathbf{k}_n) = \sum_{\alpha_1, \dots, \alpha_n} \left. \frac{\partial^n F_X}{\partial \chi_{\alpha_1} \dots \partial \chi_{\alpha_n}} \right|_{\chi_\alpha=0} U_{\alpha_1}(\mathbf{k}_1) \dots U_{\alpha_n}(\mathbf{k}_n), \quad (98)$$

where $U_\alpha(\mathbf{k})$ is the Fourier transform of $U_\alpha(\mathbf{q})$. The renormalized bias function of Eq. (83) reduces to

$$c_n^L(\mathbf{k}_1, \dots, \mathbf{k}_n) = \sum_{\alpha_1, \dots, \alpha_n} \left\langle \frac{\partial^n F_X}{\partial \chi_{\alpha_1} \dots \partial \chi_{\alpha_n}} \right\rangle U_{\alpha_1}(\mathbf{k}_1) \dots U_{\alpha_n}(\mathbf{k}_n). \quad (99)$$

In the peaks model, for example, the variables χ_α contain spatial derivatives of a smoothed density field, $\partial \delta_R / \partial q_i$, $\partial^2 \delta_R / \partial q_i \partial q_j$, and corresponding kernel windows are $U_\alpha(\mathbf{k}) = ik_i W(kR)$, $-k_i k_j W(kR)$, respectively. When one of the variables χ_α is given by the linear gravitational potential Φ_L , the kernel window U_α in Fourier space is given by $U_\alpha(\mathbf{k}) = -4\pi G a^2 \bar{\rho} / k^2$.

C. Bias functions from universal mass function

One of the most popular models of biasing in nonlinear structure formation is provided by the halo approach [53–57], which is based on the extended Press-Schechter theory [87–91]. The peak-background split is applied in this approach, and the bias of halos are considered as a local Lagrangian bias. The bias functions can be calculated by Eq. (88) or Eq. (89) in this case. In this subsection, we derive explicit expressions of the bias functions of halos. The derivation is similar to that of Ref. [75], in which the Gaussian initial conditions are assumed, and unfortunately the powers of growth factor in final expressions are incorrect. Below we correct the expressions of the last reference and give a derivation which applies even when the initial density field is non-Gaussian in general.

The mass of halo is related to the Lagrangian radius R of a spherical cell by $M = 4\pi \bar{\rho} R^3 / 3$, or $R = [M / (1.162 \times 10^{12} h^{-1} M_\odot \Omega_m)]^{1/3} h^{-1} \text{Mpc}$, where $M_\odot = 1.989 \times 10^{30} \text{kg}$ is the solar mass, and Ω_m is the density parameter at the present time. Henceforth, $\sigma^2(M)$ denotes the variance of density fluctuations smoothed on a mass scale M which is linearly extrapolated to the present time.

According to the Press-Schechter theory and its extensions, the comoving number density of halos with a mass range dM around M , identified at redshift z , is given by

$$n(M, z) dM = \frac{\bar{\rho}}{M} f_{\text{MF}}(\nu) d \ln \nu, \quad (100)$$

where $\nu = \delta_c(z) / \sigma(M)$ is the typical amplitude of fluctuations that produce those halos, $\delta_c(z) = \Delta_c / D(z)$, and Δ_c is the critical overdensity for spherical collapse at the redshift z . In the Einstein-de Sitter model, the critical overdensity is independent on redshift, $\Delta_c = 3(3\pi/2)^{2/3} / 5 \simeq 1.686$, and only weakly depends on cosmological parameters and redshift in general cosmology. Since the condition of collapse is always expressed by the linearly extrapolated overdensity at the present

time, the growth factor is absorbed into the critical overdensity $\delta_c(z)$. The multiplicity function $f_{\text{MF}}(\nu)$ is normalized by

$$\int_0^\infty f_{\text{MF}}(\nu) \frac{d\nu}{\nu} = 1, \quad (101)$$

to ensure all the mass in the universe is contained in halos in the limit $D(z) \rightarrow \infty$.

In the original Press-Schechter (PS) theory, the multiplicity function $f_{\text{MF}}(\nu)$ is given by

$$f_{\text{PS}}(\nu) = \sqrt{\frac{2}{\pi}} \nu e^{-\nu^2/2}. \quad (102)$$

The original PS mass function is improved by Sheth and Tormen (ST) [55] to give a better fit in numerical simulations of CDM-type cosmologies with Gaussian initial conditions. The corresponding multiplicity function is given by

$$f_{\text{ST}}(\nu) = A(p) \sqrt{\frac{2}{\pi}} \left[1 + \frac{1}{(q\nu^2)^p} \right] \sqrt{q} \nu e^{-q\nu^2/2}, \quad (103)$$

where $p = 0.3$, $q = 0.707$ are numerically fitted parameters, and $A(p) = [1 + \pi^{-1/2} 2^{-p} \Gamma(1/2 - p)]^{-1}$ is the normalization factor. The ST mass function is applicable only for Gaussian initial conditions. When the non-Gaussianity is present in the initial density field, the multiplicity function should have the correction factor [92, 93].

In the extended PS theory, the number density of halos of mass M , identified at redshift z , in a region of Lagrangian radius R_0 in which the linear overdensity extrapolated to the present time is δ_0 , is given by [57]

$$n(M, z | \delta_0, R_0) dM = \frac{\bar{\rho}}{M} f_{\text{MF}}(\nu') d \ln \nu', \quad (104)$$

where

$$\nu' = \frac{\delta_c(z) - \delta_0}{[\sigma^2(M) - \sigma_0^2]^{1/2}}, \quad \sigma_0 = \sigma(M_0), \quad M_0 = 4\pi \bar{\rho} R_0^3 / 3. \quad (105)$$

The halo of mass M is collapsed at z , while M_0 is assumed uncollapsed at $z = 0$, and thus we always have $\delta_c(z) > \delta_0$. The conditional number density of Eq. (104) represents the biasing for the Lagrangian number density of halos. The smoothed density contrast δ_0 of mass modulates the number of halos. The density contrast of halos in Lagrangian space is given by

$$\delta_h^L = \frac{n(M, z | \delta_0, R_0)}{n(M, z)} - 1. \quad (106)$$

Since $d \ln \nu' / d \ln \nu = \sigma^2(M) / [\sigma^2(M) - \sigma_0^2]$, we have

$$\delta_h^L = \frac{\sigma^2(M)}{\sigma^2(M) - \sigma_0^2} \frac{f_{\text{MF}}(\nu')}{f_{\text{MF}}(\nu)} - 1. \quad (107)$$

This relation gives the function $F_X(\delta_R)$ of Eq. (86), where the smoothing radius in Eq. (86) correspond to $R \rightarrow R_0$ here. We assume the redshift z of halo identification is the same as the redshift of halo observation. The smoothed linear density field

in Eq. (86) corresponds to $\delta_R \rightarrow D(z)\delta_0$ here, because δ_0 is the value extrapolated to the present time.

To evaluate the bias functions, the derivatives $F_X^{(n)}$ in Eqs. (88), (89) need to be derived. We consider a limit of the peak-background split for simplicity, and assume $\sigma^2(M) \gg \sigma_0^2$ (However, see Ref. [94] for limitations of this commonly used method.). In this limit, we have

$$F_X^{(n)}(\delta_R) \simeq \frac{1}{D^n(z)} \left(\frac{\partial}{\partial \delta_0} \right)^n \delta_h^L = \left(\frac{-1}{D(z)\sigma(M)} \right)^n \frac{f_{MF}^{(n)}(\nu')}{f_{MF}(\nu)}, \quad (108)$$

for $n \geq 1$, where $f_{MF}^{(n)}$ is the n -th derivative of the multiplicity function f_{MF} . The substitution $\delta_0 = 0$ is equivalent to $\nu' = \nu$ in the present limit. In the same limit, taking the statistical average over the distribution of δ_0 also equivalent to substituting $\nu' = \nu$ in Eq. (108), because the distribution function of δ_0 is highly peaked at $\delta_0 = 0$ and its variance is much smaller than $\delta_c^2(z)$. Therefore, we have

$$F_X^{(n)}(0) \simeq \langle F_X^{(n)}(\delta_R) \rangle \simeq \left(\frac{-1}{D(z)\sigma(M)} \right)^n \frac{f_{MF}^{(n)}(\nu)}{f_{MF}(\nu)}, \quad (109)$$

in the limit of peak-background split, $\sigma^2(M) \gg \sigma_0^2$. The Lagrangian bias functions of Eqs. (88), (89) reduces to

$$b_n^L(\mathbf{k}_1, \dots, \mathbf{k}_n) = c_n^L(\mathbf{k}_1, \dots, \mathbf{k}_n) = \left(\frac{-1}{D(z)\sigma(M)} \right)^n \frac{f_{MF}^{(n)}(\nu)}{f_{MF}(\nu)}, \quad (110)$$

where the window function to define the background field δ_0 is dropped, assuming the large-scale limit $|\mathbf{k}_i| \ll 1/R_0$. The last approximation is consistent with that of the peak-background split. The above Eq. (110) is applicable even in non-Gaussian initial conditions, as long as effects of non-Gaussianity are taken into account in the multiplicity function.

In the case of ST mass function of Eq. (103) with Gaussian initial conditions, the above bias functions are given by

$$b_1^L = \frac{1}{\Delta_c} \left[qv^2 - 1 + \frac{2p}{1 + (qv^2)^p} \right], \quad (111)$$

$$b_2^L = \frac{1}{\Delta_c^2} \left[q^2 v^4 - 3qv^2 + \frac{2p(2qv^2 + 2p - 1)}{1 + (qv^2)^p} \right], \quad (112)$$

and so forth. Essentially the same expressions are derived in Ref. [75]. Unfortunately, the factor $1/D^n(z)$ is incorrectly missing in Eq. (55) of Ref. [75]. Accordingly, the factor $\delta_c(z)$ which appear in Eqs. (57)–(59) of that paper should be replaced by $\Delta_c = D(z)\delta_c(z)$.

D. Some properties of peaks bias

In the peaks formalism, a density peak in Lagrangian space is considered as a location of structure formation [60]. In the smoothed density field $\delta_R(\mathbf{q})$, the number density of peaks above a height ν is given by

$$n_{pk} = \theta(\delta_R/\sigma_R - \nu) \delta_D^3(\nabla\delta_R) |\det(\nabla\nabla\delta_R)| \theta(\lambda_3) \quad (113)$$

where $\sigma_R = \langle \delta_R^2 \rangle^{1/2}$, and λ_3 is the smallest eigenvalue of the matrix $[-\nabla\nabla\delta_R]_{ij} = -\partial_i\partial_j\delta_R$. Thus the number density of peaks is a multivariate function of a scalar δ_R , a vector $\nabla\delta_R$, and a tensor $\nabla\nabla\delta_R$ at each position.

The number density of Eq. (113) is a singular function. Therefore the Taylor expansion cannot be applied. The unrenormalized bias functions b_n are not well-defined in this case, and it is crucial to consider the renormalized bias functions of Eq. (83). The peaks bias is one of the multivariate Lagrangian bias as described in Sec. VB, and the renormalized bias function is given by Eq. (99) where $(\chi_\alpha) = (\delta_R, \nabla\delta_R, \nabla\nabla\delta_R)$ is a 10-dimensional vector. Since $\nabla\nabla\delta_R$ is a symmetric tensor, only six components of $\partial_i\partial_j\delta_R$ are independent. The corresponding kernels in Eq. (96) are given by $(U_\alpha) = [W(kR), ik_iW(kR), -k_i k_j W(kR)]$ where $i \leq j$.

The calculation of the coefficient $\langle \partial^n F_X / \partial \chi_{\alpha_1} \cdots \partial \chi_{\alpha_n} \rangle$ for general n in the peaks model is quite involved. In Ref. [62, 64], the correlation function and the power spectrum of peaks are calculated up to second order in the case of Gaussian initial condition. In this paper, we do not derive explicit forms of the coefficients. Instead, we consider formal properties of the bias functions derived from the rotational symmetry below.

For $n = 1$, we have

$$c_1^L(\mathbf{k}) = W(kR) \left[\left\langle \frac{\partial F_X}{\partial \delta_R} \right\rangle + i \sum_i k_i \left\langle \frac{\partial F_X}{\partial \delta_{R,i}} \right\rangle - \sum_{i,j} k_i k_j \left\langle \frac{\partial F_X}{\partial \delta_{R,ij}} \right\rangle \right], \quad (114)$$

where $\delta_{R,i} = \partial_i\delta_R$ and $\delta_{R,ij} = \partial_i\partial_j\delta_R$. In the above equation, the function F_X is symmetrized with respect to the off-diagonal derivatives $\partial_i\partial_j\delta_R$, and partial derivatives are taken as if $\partial_i\partial_j\delta_R$ and $\partial_j\partial_i\delta_R$ were independent when $i \neq j$. From the rotational symmetry, the second term in the square parenthesis in Eq. (114) identically vanishes. The last term is proportional to k^2 , since $\langle \partial F_X / \partial \delta_{R,ij} \rangle \propto \delta_{ij}$. Thus, the scale dependence of the first-order bias function should have a form,

$$c_1^L(\mathbf{k}) = W(kR) (A_1 + B_1 k^2), \quad (115)$$

where

$$A_1 = \left\langle \frac{\partial F_X}{\partial \delta_R} \right\rangle, \quad B_1 = -\frac{1}{3} \sum_i \left\langle \frac{\partial F_X}{\partial \delta_{R,ii}} \right\rangle. \quad (116)$$

This form is exact for peaks bias models [64, 70], and higher-order powers of k^n with $n \geq 3$ do not appear.

It is easily understood that the first bias function of peaks should have the form of Eq. (115). The peaks are defined by up to second derivatives of the smoothed field, and thus the first bias functions of Eqs. (98), (99) involve only polynomials of wavevector \mathbf{k} up to second order. Since the bias function is rotationally invariant, only the form of Eq. (115) is allowed.

For $n = 2$, the same considerations show that the bias function should have a form,

$$c_2^L(\mathbf{k}_1, \mathbf{k}_2) = W(k_1 R) W(k_2 R) \left[A_2 + B_2 (k_1^2 + k_2^2) + C_2 \mathbf{k}_1 \cdot \mathbf{k}_2 + D_2 k_1^2 k_2^2 + E_2 (\mathbf{k}_1 \cdot \mathbf{k}_2)^2 \right], \quad (117)$$

where

$$A_2 = \left\langle \frac{\partial^2 F_X}{\partial \delta_R^2} \right\rangle, \quad (118)$$

$$B_2 = -\frac{1}{3} \sum_i \left\langle \frac{\partial^2 F_X}{\partial \delta_R \partial \delta_{R,ii}} \right\rangle, \quad (119)$$

$$C_2 = -\frac{1}{3} \sum_i \left\langle \frac{\partial^2 F_X}{\partial \delta_{R,i}^2} \right\rangle, \quad (120)$$

$$D_2 = \frac{2}{15} \sum_{i,j} \left\langle \frac{\partial^2 F_X}{\partial \delta_{R,ii} \partial \delta_{R,jj}} \right\rangle - \frac{1}{15} \sum_{i,j} \left\langle \frac{\partial^2 F_X}{\partial \delta_{R,ij}^2} \right\rangle, \quad (121)$$

$$E_2 = -\frac{1}{30} \sum_{i,j} \left\langle \frac{\partial^2 F_X}{\partial \delta_{R,ii} \partial \delta_{R,jj}} \right\rangle + \frac{1}{10} \sum_{i,j} \left\langle \frac{\partial^2 F_X}{\partial \delta_{R,ij}^2} \right\rangle. \quad (122)$$

It is again easily understood that the second bias function of peaks should have the form of Eq. (117), since the function is rotationally invariant and made from polynomials of wavevectors \mathbf{k}_1 and \mathbf{k}_2 up to second order for each. The explicit evaluations of the above coefficients are tedious. In Ref. [64], second-order biased correlation function with a Gaussian initial condition is analytically calculated. Similar techniques should be also useful in our formalism, which we leave for future work.

VI. CONCLUSIONS

In this paper, the standard nonlinear perturbation theory of the gravitational instability is extended in several directions. One of the main extensions is the inclusion of the nonlocal bias, which is a general framework of biasing. Nonlocal biases both in Eulerian and Lagrangian spaces are formulated and consistently included in EPT and LPT, respectively. The nonlinear Eulerian and Lagrangian biases are compatible only in the framework of nonlocal bias. The relations among perturbation kernels of EPT and LPT with nonlocal biases are derived.

Effects of redshift-space distortions and primordial non-Gaussianity are also included in our formalism. Therefore, our formalism provides a complete theory to predict the observable quantities in redshift surveys, once a model of bias and cosmology are given.

The concept of vertex resummations in the presence of nonlocal bias is introduced. We show that the vertex resummation of the bias extends the applicability of the formalism to the case when the bias function(al) cannot be expanded into a Taylor series. This extension is essential for handling, e.g., the threshold bias and the peaks model, in which the bias involves singular functions such as the Heaviside's step function, Dirac's delta function, etc. Calculation of perturbative bias functions in our formalism is exemplified by considering some models of local and nonlocal models of Lagrangian bias, such as the threshold bias model, the multivariate bias model, the halo model, and the peaks model. The scale dependence of bias functions are straightforwardly obtained in our formalism once a model of nonlocal bias is given. The scale dependence

of Eulerian bias arises both from the nonlocal Lagrangian bias and nonlinear evolutions.

The formalism of the present paper provides a basic methodology for future applications of the perturbation theory. For example, the scale-dependent bias in the presence of primordial non-Gaussianity has been derived by adopting either halo models [7–9] or the local Eulerian bias [10]. Our formalism allows to calculate the scale-dependent bias in any models of bias in a consistent manner [95]. The power spectrum with BAO in any given models of bias can be calculated with our formalism. The result of applying our formalism to a local Lagrangian bias is equivalent to the work in Ref. [75]. More precise modeling of the bias would be required in future analysis of the BAO in the galaxy power spectrum to constrain the nature of dark energy.

Our formalism provides a way to perturbatively calculate the nonlinear power spectrum, bispectrum, trispectrum, and other polyspectra. These polyspectra are fundamental statistics and any other statistics in the large-scale structure, such as the correlation functions, counts-in-cells, genus statistics, etc. are expressible by these polyspectra, in principle. The formalism developed in this paper would have an essential importance in the era of precision cosmology with the large-scale structure of the universe.

Acknowledgments

I wish to thank R. Sheth for helpful discussion. I acknowledge support from the Ministry of Education, Culture, Sports, Science, and Technology, Grant-in-Aid for Scientific Research (C), 21540263, 2009, and Grant-in-Aid for Scientific Research on Priority Areas No. 467 “Probing the Dark Energy through an Extremely Wide and Deep Survey with Subaru Telescope.” This work is supported in part by JSPS (Japan Society for Promotion of Science) Core-to-Core Program “International Research Network for Dark Energy.”

Appendix A: Bias Parameters in the Spherical Collapse Model

In this Appendix, the relations between the Eulerian and Lagrangian bias parameters in the spherical collapse model are derived, following and generalizing the argument of Ref. [54]. The Einstein–de Sitter universe is assumed in the following equations for simplicity. The dependences of the results on cosmological parameters are weak.

The time evolution of proper radius r for a spherical mass shell as a function of the scale factor a is given by a parametric form [12]

$$\frac{r}{r_i} = \frac{3}{10} \frac{1 - \cos \theta}{\delta_i}, \quad (A1)$$

$$\frac{a}{a_i} = \frac{3}{10} \left(\frac{9}{2} \right)^{1/3} \frac{(\theta - \sin \theta)^{2/3}}{\delta_i}, \quad (A2)$$

where r_i and a_i are initial values of r and a , respectively, and δ_i is the initial density contrast at a_i . For $\delta_i > 0$, the parameter

θ is a positive real number. For $\delta_i < 0$, the replacement $\theta \rightarrow i\theta$ should be applied to have the parameter real and positive.

The comoving radius is given by $R = r/a$, and therefore an overdensity $\rho/\bar{\rho}$ of any kind in the spherical volume is enhanced by a factor of $(R_i/R)^3 = (a/a_i)^3(r_i/r)^3 = (9/2)(\theta - \sin \theta)^2/(1 - \cos \theta)^3$. Thus, the density contrasts of mass δ_m and of biased object δ_X in the spherical volume are given by $1 + \delta_m = (R_i/R)^3$ in the limit of $|\delta_i| \ll 1$, and $1 + \delta_X = (R_i/R)^3(1 + \delta_X^L)$, where δ_X^L is the density contrast in Lagrangian space. Thus, we have

$$1 + \delta_m = \frac{9}{2} \frac{(\theta - \sin \theta)^2}{(1 - \cos \theta)^3}, \quad (\text{A3})$$

$$1 + \delta_X = (1 + \delta_m)(1 + \delta_X^L). \quad (\text{A4})$$

The form of Eq. (A3) is well-known [12]. The Eq. (A4) can also be derived from general Eqs. (16) and (17) in the case of spherical perturbations.

The linear density contrast δ_L is proportional to the scale factor a , and from Eq. (A2), we have

$$\delta_L = \frac{3}{10} \left(\frac{9}{2} \right)^{1/3} (\theta - \sin \theta)^{2/3}. \quad (\text{A5})$$

For $|\delta_m| \ll 1$, the relation between δ_m and δ_L is derived as a power series by Taylor expansions of Eqs. (A3) and (A5) with respect to the parameter θ . The results are

$$\delta_m = \delta_L + \frac{17}{21} \delta_L^2 + \frac{341}{567} \delta_L^3 + \frac{55805}{130977} \delta_L^4 + \dots, \quad (\text{A6})$$

$$\delta_L = \delta_m - \frac{17}{21} \delta_m^2 + \frac{2815}{3969} \delta_m^3 - \frac{590725}{916839} \delta_m^4 + \dots. \quad (\text{A7})$$

The Eq. (A6) is derived in Ref. [96]. Although the Eq. (A7) is described in Refs. [54, 57], they put incorrect numbers in the coefficients of third- and fourth-order terms. The coefficients a_3 and a_4 in their Eq. (A4) of Ref. [54] should be replaced by $a_3 = 2815/3969$ and $a_4 = -590725/916839$.

The dynamical evolutions are local in the spherical collapse model. In this special case, both the Eulerian and Lagrangian biases can be simultaneously local. We have expansions

$$\delta_X = \sum_{n=1}^{\infty} \frac{b_n}{n!} \delta_m^n, \quad (\text{A8})$$

$$\delta_X^L = \sum_{n=1}^{\infty} \frac{b_n^L}{n!} \delta_L^n, \quad (\text{A9})$$

where b_n and b_n^L are constant bias parameters. Putting Eqs. (A4), (A7), (A9) together, we have a series expansion of δ_X in terms of δ_m . Equating the resulting coefficients with Eq. (A8) gives

$$b_1 = b_1^L + 1, \quad (\text{A10})$$

$$b_2 = b_2^L + \frac{8}{21} b_1^L, \quad (\text{A11})$$

$$b_3 = b_3^L - \frac{13}{7} b_2^L - \frac{796}{1323} b_1^L, \quad (\text{A12})$$

$$b_4 = b_4^L - \frac{40}{7} b_3^L + \frac{7220}{1323} b_2^L + \frac{476320}{305613} b_1^L. \quad (\text{A13})$$

Since the relation of Eq. (A7) depends only very weakly on cosmological model [96], the relations of Eqs. (A10)–(A13) also do so.

-
- [1] C. Alcock and B. Paczynski, *Nature (London)* , **281**, 358 (1979).
 - [2] W. E. Ballinger, J. A. Peacock, and A. F. Heavens, *Mon. Not. R. Astron. Soc.* , **282**, 877 (1996).
 - [3] T. Matsubara and Y. Suto, *Astrophys. J. Letters* , **470**, L1 (1996).
 - [4] D. J. Eisenstein, W. Hu, and M. Tegmark, *Astrophys. J. Letters* , **504**, L57 (1998).
 - [5] T. Matsubara, *Astrophys. J.* , **615**, 573 (2004).
 - [6] D. J. Eisenstein et al., *Astrophys. J.* **633**, 560 (2005);
 - [7] N. Dalal, O. Doré, D. Huterer and A. Shirokov, *Phys. Rev. D* , **77**, 123514 (2008).
 - [8] S. Matarrese and L. Verde, *Astrophys. J. Letters* , **677**, L77 (2008).
 - [9] A. Slosar, C. Hirata, U. Seljak, S. Ho, N. Padmanabhan, *J. Cosmol. Astropart. Phys.* , **8**, 31 (2008).
 - [10] A. Taruya, K. Koyama and T. Matsubara, *Phys. Rev. D* , **78**, 123534 (2008).
 - [11] V. Desjacques, U. Seljak and I. T. Iliev, *Mon. Not. R. Astron. Soc.* , **396**, 85 (2009).
 - [12] P. J. E. Peebles, *The Large-Scale Structure of the Universe* (Princeton University, Princeton, NJ, 1980).
 - [13] R. Juszkiewicz, *Mon. Not. R. Astron. Soc.* , **197**, 931 (1981).
 - [14] E. T. Vishniac, *Mon. Not. R. Astron. Soc.* , **203**, 345 (1983).
 - [15] J. N. Fry, *Astrophys. J.* , **279**, 499 (1984).
 - [16] M. H. Goroff, B. Grinstein, S.-J. Rey, and M. B. Wise, *Astrophys. J.* , **311**, 6 (1986).
 - [17] Y. Suto, M. Sasaki, *Phys. Rev. Lett.* , **66**, 264 (1991). N. Makino, M. Sasaki, and Y. Suto, *Phys. Rev. D* , **46**, 585 (1992).
 - [18] B. Jain and E. Bertschinger, *Astrophys. J.* , **431**, 495 (1994).
 - [19] R. Scoccimarro and J. Frieman, *Astrophys. J. Suppl. Ser.* , **105**, 37 (1996).
 - [20] F. Bernardeau, S. Colombi, E. Gaztañaga, and R. Scoccimarro, *Phys. Rep.* , **367**, 1 (2002).
 - [21] T. Buchert, *Astron. Astrophys.* , **223**, 9 (1989).
 - [22] F. Moutarde, J.-M. Alimi, F. R. Bouchet, R. Pellat, and A. Rami, *Astrophys. J.* , **382**, 377 (1991).
 - [23] T. Buchert, *Mon. Not. R. Astron. Soc.* , **254**, 729 (1992).
 - [24] T. Buchert and J. Ehlers, *Mon. Not. R. Astron. Soc.* , **264**, 375 (1993).
 - [25] T. Buchert, *Mon. Not. R. Astron. Soc.* , **267**, 811 (1994).
 - [26] E. Hivon, F. R. Bouchet, S. Colombi and R. Juszkiewicz, *Astron. Astrophys.* , **298**, 643 (1995).
 - [27] P. Catelan, *Mon. Not. R. Astron. Soc.* , **276**, 115 (1995).
 - [28] P. Catelan and T. Theuns, *Mon. Not. R. Astron. Soc.* , **282**, 455 (1996).
 - [29] J. Ehlers and T. Buchert, *General Relativity and Gravitation* , **29**,

- 733 (1997).
- [30] Ya. B. Zel'dovich, *Astron. Astrophys.*, **5**, 84 (1970)
- [31] M. Crocce and R. Scoccimarro, *Phys. Rev. D*, **73**, 063519 (2006).
- [32] M. Crocce and R. Scoccimarro, *Phys. Rev. D*, **73**, 063520 (2006).
- [33] P. McDonald, *Phys. Rev. D*, **75**, 043514 (2007).
- [34] P. Valageas, *Astron. Astrophys.*, **465**, 725 (2007). (2008).
- [35] S. Matarrese and M. Pietroni, *J. Cosmol. Astropart. Phys.*, 0706 (2007) 026.
- [36] S. Matarrese and M. Pietroni, *Mod. Phys. Lett. A*, **23**, 25 (2008)
- [37] A. Taruya and T. Hiramatsu, *Astrophys. J.*, **674**, 617 (2008).
- [38] M. Pietroni, *J. Cosmol. Astropart. Phys.*, **10**, 36 (2008)
- [39] T. Matsubara, *Phys. Rev. D*, **77**, 063530 (2008)
- [40] R. Scoccimarro, *Ann. N.Y. Acad. Sci.* **927**, 13 (2001).
- [41] N. Kaiser, *Mon. Not. R. Astron. Soc.*, **227**, 1 (1987).
- [42] A. J. S. Hamilton, *Astrophys. J. Letters*, **385**, L5 (1992).
- [43] A. F. Heavens, S. Matarrese, and L. Verde, *Mon. Not. R. Astron. Soc.*, **301**, 797 (1998).
- [44] R. Scoccimarro, H. M. P. Couchman, and J. A. Frieman, *Astrophys. J.*, **517**, 531 (1999)
- [45] J. C. Jackson, *Mon. Not. R. Astron. Soc.*, **156**, 1P (1972)
- [46] W. L. W. Sargent and E. L. Turner, *Astrophys. J. Letters*, **212**, L3 (1977).
- [47] J. A. Peacock and S. J. Dodds, *Mon. Not. R. Astron. Soc.*, **267**, 1020 (1994).
- [48] R. Scoccimarro, *Phys. Rev. D*, **70**, 083007 (2004)
- [49] A. Taruya, T. Nishimichi and S. Saito, *Phys. Rev. D*, **82**, 063522 (2010).
- [50] P. Coles, *Mon. Not. R. Astron. Soc.*, **262**, 1065 (1993).
- [51] J. N. Fry and E. Gaztanaga, *Astrophys. J.*, **413**, 447 (1993).
- [52] R. J. Scherrer and D. H. Weinberg, *Astrophys. J.*, **504**, 607 (1998)
- [53] H. J. Mo and S. D. M. White, *Mon. Not. R. Astron. Soc.*, **282**, 347 (1996).
- [54] H. J. Mo, Y. P. Jing, and S. D. M. White, *Mon. Not. R. Astron. Soc.*, **284**, 189 (1997).
- [55] R. K. Sheth and G. Tormen, *Mon. Not. R. Astron. Soc.*, **308**, 119 (1999). (2000).
- [56] R. Scoccimarro, R. K. Sheth, L. Hui, and B. Jain, *Astrophys. J.*, **546**, 20 (2001).
- [57] A. Cooray and R. Sheth, *Phys. Rep.*, **372**, 1 (2002).
- [58] N. Kaiser, *Astrophys. J. Letters*, **284**, L9 (1984).
- [59] M. Davis, G. Efstathiou, C. S. Frenk, and S. D. M. White, *Astrophys. J.*, **292**, 371 (1985).
- [60] J. Bardeen, J. R. Bond, N. Kaiser, and A. S. Szalay, *Astrophys. J.*, **304**, 15 (1986).
- [61] E. Regos and A. S. Szalay, *Mon. Not. R. Astron. Soc.*, **272**, 447 (1995).
- [62] V. Desjacques, *Phys. Rev. D*, **78**, 103503 (2008).
- [63] V. Desjacques and R. K. Sheth, *Phys. Rev. D*, **81**, 023526 (2010).
- [64] V. Desjacques, M. Crocce, R. Scoccimarro and R. K. Sheth, *Phys. Rev. D*, **82**, 103529 (2010).
- [65] A. Taruya, *Astrophys. J.*, **537**, 37 (2000).
- [66] P. McDonald, *Phys. Rev. D*, **74**, 103512 (2006); **74**, 129901(E) (2006).
- [67] D. Jeong and E. Komatsu, *Astrophys. J.*, **691**, 569 (2009).
- [68] A. J. Benson, *Phys. Rep.*, **495**, 33 (2010).
- [69] A. Dekel and O. Lahav, *Astrophys. J.*, **520**, 24 (1999).
- [70] T. Matsubara, *Astrophys. J.*, **525**, 543 (1999).
- [71] T. Matsubara, *Astrophys. J.*, **535**, 1 (2000).
- [72] A. N. Taylor and A. J. S. Hamilton, *Mon. Not. R. Astron. Soc.*, **282**, 767 (1996)
- [73] F. Bernardeau, M. Crocce and R. Scoccimarro, *Phys. Rev. D*, **78**, 103521 (2008)
- [74] F. Bernardeau, M. Crocce and E. Sefusatti, *Phys. Rev. D*, **82**, 083507 (2010)
- [75] T. Matsubara, *Phys. Rev. D*, **78**, 083519 (2008); **78**, 109901(E) (2008)
- [76] A. Elia, S. Kulkarni, C. Porciani, M. Pietroni and S. Matarrese, arXiv:1012.4833.
- [77] T. Matsubara, *Astrophys. J. Suppl. Ser.*, **101**, 1 (1995)
- [78] S.-K. Ma, *Statistical Mechanics* (World Scientific, Singapore, 1985), Sec. 12
- [79] M. Crocce and R. Scoccimarro, *Phys. Rev. D*, **77**, 023533 (2008).
- [80] H. D. Politzer, and M. B. Wise, *Astrophys. J. Letters*, **285**, L1 (1984).
- [81] L. G. Jensen, and A. S. Szalay, *Astrophys. J. Letters*, **305**, L5 (1986).
- [82] S. Matarrese, F. Lucchin, and S. A. Bonometto, *Astrophys. J. Letters*, **310**, L21 (1986).
- [83] P. McDonald, *Phys. Rev. D*, **78**, 123519 (2008). m
- [84] T. Giannantonio, and C. Porciani, *Phys. Rev. D*, **81**, 063530 (2010).
- [85] T. Baldauf, U. Seljak, and L. Senatore, arXiv:1011.1513 (2010).
- [86] P. McDonald and A. Roy, *J. Cosmol. Astropart. Phys.*, **8**, 20 (2009).
- [87] W. H. Press and P. Schechter, *Astrophys. J.*, **187**, 425 (1974).
- [88] R. I. Epstein, *Mon. Not. R. Astron. Soc.*, **205**, 207 (1983).
- [89] J. A. Peacock and A. F. Heavens, *Mon. Not. R. Astron. Soc.*, **243**, 133 (1990).
- [90] R. G. Bower, *Mon. Not. R. Astron. Soc.*, **248**, 332 (1991).
- [91] J. R. Bond, S. Cole, G. Efstathiou, and N. Kaiser, *Astrophys. J.*, **379**, 440 (1991).
- [92] S. Matarrese, L. Verde and R. Jimenez, *Astrophys. J.*, **541**, 10 (2000).
- [93] M. Lo Verde, A. Miller, S. Shandera and L. Verde, *J. Cosmol. Astropart. Phys.*, **4**, 14 (2008).
- [94] M. Manera, R. K. Sheth and R. Scoccimarro, *Mon. Not. R. Astron. Soc.*, **402**, 589 (2010).
- [95] T. Matsubara, in preparation.
- [96] F. Bernardeau, *Astrophys. J.*, **392**, 1 (1992).